Convective distribution of dust over the Arabian Peninsula: the impact of model resolution

Jennie Bukowski[1], Susan C. van den Heever[1]

[1] Department of Atmospheric Science, Colorado State University, Fort Collins, CO

Correspondence to: Jennie Bukowski (jennie.bukowski@colostate.edu)

Abstract

Along the coasts of the Arabian Peninsula, convective dust storms are a considerable source of mineral dust to the atmosphere. Reliable predictions of convective dust events are necessary to determine their effects on air quality, visibility, and the radiation budget. In this study, the Weather Research and Forecasting Model coupled with Chemistry (WRF-Chem) is used to simulate a 2016 summertime dust event over the Arabian Peninsula and examine the variability in dust fields and associated vertical transport due to the choice of convective parameterization and convection-allowing versus parameterized convection. Simulations are run at 45 km and 15 km grid spacing with multiple cumulus parameterizations, and are compared to a 3 km simulation that permits explicit dry and moist convective processes. Five separate cumulus parameterizations at 15 km grid spacing were tested to quantify the spread across different parameterizations. Finally, the impact these variations have on radiation, specifically aerosol heating rates is also investigated.

On average, in these simulations the convection-permitting case produces higher quantities of dust than the parameterized cases in terms of dust uplift potential, vertical dust concentrations, and vertical dust fluxes. Major drivers of this discrepancy between the simulations stem from the convection-allowing case exhibiting higher surface windspeeds during convective activity, lower dust emission wind threshold velocities due to drier soil, and more frequent, stronger vertical velocities which transport dust aloft and increase the atmospheric lifetime of these particles. For aerosol heating rates in the lowest levels, the shortwave effect prevails in the convection-permitting case with a net cooling effect, whereas a longwave net warming effect is present in the parameterized cases. The spread in dust concentrations across cumulus parameterizations at the same grid resolution (15 km) is an order of magnitude lower than the impact of moving from parameterized towards explicit convection. We conclude that tuning dust emissions in coarse resolution simulations can only improve the results to first-order and cannot fully rectify the discrepancies originating from disparities in the representation of convective dust transport.

1) Introduction

Airborne mineral dust is an important atmospheric aerosol (Zender et al., 2004; Ginoux et al., 2012): dust reduces visibility (e.g. Mahowald et al., 2007; Baddock et al., 2014; Camino et al., 2015) and is detrimental to the human respiratory system (Prospero, 1999; van Donkelaar et al., 2010; Stafoggia et al., 2016), but also plays a vital role in

32   fertilizing iron-deficient maritime ecosystems (Martin, 1991; Bishop et al., 2002; Mahowald et al., 2005; Jickells

33   and Moore, 2015). Dust particles function as cloud condensation nuclei (e.g. Lee et al., 2009; Manktelow et al.,

34   2009; Twohy et al., 2009; Karydis et al., 2011) and ice nuclei (e.g. DeMott et al., 2003; Field et al., 2006; Knopf and

35   Koop, 2006; Boose et al., 2016), thereby altering cloud development and properties. Furthermore, mineral dust is of

36   interest due to its distinctive optical properties; dust both scatters and absorbs shortwave and longwave radiation

37   (e.g. Tegen et al., 1996; Kinne et al., 2003; Dubovik et al., 2006) modifying atmospheric thermodynamics and the

38   earth's energy budget in the process (e.g. Slingo et al., 2006; Sokolik and Toon, 2006; Heald et al., 2014).

39   The influence of atmospheric mineral dust is widespread in the weather and climate system, yet generating skillful

40   forecasts of dust concentrations and their temporal and spatial evolution has been difficult to achieve. Several

41   studies suggest that including the radiative effects of mineral dust in numerical weather prediction (NWP) could

42   refine the radiation balance of these models and improve forecasts (Kischa et al., 2003; Haywood et al., 2005; Pérez

43   et al., 2006). Advances in climate models have been made by incorporating time-varying dust sources and climate-

44   dust feedbacks in the radiative forcing calculations (Kok et al., 2014; Woodage and Woodward, 2014; Kok et al.,

45   2018). However, these potential improvements are contingent upon ingesting both vertical dust concentrations from

46   models or observations at simulation initialization, as well as correctly representing the coupled radiative effect dust

47   has on the atmosphere. Even the state-of-the-art models are currently incapable of this type of assimilation and rely

48   on the quality of the dust model and initialization data, which models are known to be especially sensitive to and

49   will vary depending on the specific region and case study. As such, substantial discrepancies exist across global

50   models of similar resolution (Huneeus et al., 2011), and across regional models (Uno et al., 2006; Todd et al., 2008)

51   in the magnitude of predicted dust flux from the surface to the atmosphere, as well as the models' overall

52   representation of the dust cycle.

53   A major challenge in modeling dust processes is the scales of motion involved in its emission and subsequent

54   transport. Dust particles mobilize from the surface due to wind erosion of arid soils, a mechanism that occurs on the

55   micron scale and must be parameterized in numerical models. Once airborne, mineral dust can deposit locally or be

56   transported on the synoptic to global scales. Dust events initiate from both large-scale and synoptic dynamical flow

57   regimes, as well as mesoscale features. Synoptic scale uplift phenomena include monsoon troughs (e.g. Marsham et

58   al., 2008), Shamal winds (e.g. Yu et al., 2015) and frontal systems (e.g. Beegum et al. 2018), while dynamical

59   effects on smaller (meso) scales can raise dust through the production of convective outflow boundaries, or haboobs,

60   (e.g. Miller et al. 2008), daytime turbulence or dry convective processes (e.g. Klose and Shao, 2012), and the

61   morning mixing of nocturnal low level jet (NLLJ) momentum to the surface (e.g. Fiedler et al. 2013). When

62   considering only meteorological dust sources, wind drives dust emissions, meaning that the underlying processes

63   that contribute to the wind fields must be resolved in a model to create an accurate dust forecast.

64   One potential source of disagreement in models stems from the scaling emissions in dust parameterizations, which

65   relate the surface emissions proportionally to the second or third power of surface windspeed. This means that minor

66   miscalculations in modeled windspeeds go on to produce more substantial errors in the dust concentration

67 calculations (e.g. Menut, 2008). Current aerosol forecast and climate models are run at fine enough grid-spacing to
68 simulate synoptic events but still typically employ cumulus parameterizations, which are incapable of resolving dry
69 and moist mesoscale updrafts and downdrafts that can potentially loft and / or scavenge dust. Schepanski et al. 2015
70 found that online dust models are likely to be most sensitive to the initialization data compared to other model
71 options, model sensitivity to the representation of convection will be an additional source of uncertainty in dust
72 forecasts. Pope et al. (2016) and Largeron et al. (2015) both postulated that an inadequate representation of
73 convection in coarse model simulations, specifically the underestimation of high surface windspeeds in mesoscale
74 haboobs, is a major contributor to errors in dust models.

75

76 The misrepresentation of dust concentrations in models with cumulus parameterizations has been investigated across
77 several modeling platforms, mostly from the perspective of dust lofting mechanisms at the surface. Heinold et al.
78 (2013) ran the UK Met Office Unified Model (UM) over West Africa with offline dust emissions, and found that of
79 the factors they tested, the model was most sensitive to explicit versus parameterized convection. Furthermore, in
80 the Heinhold et al. (2013) study, dust emissions were reduced as grid resolution was increased to convection-
81 permitting scales by roughly 50%. This was found to be due to the parameterized simulations underestimating moist
82 convective activity but drastically overestimating the NLLJ dust uplift mechanism, a similar relationship to that
83 originally identified in Marsham et al. (2011).

84 Conversely, studies using different numerical dust models have identified other relationships between horizontal
85 resolution and dust emissions. Roberts et al. 2018 also used UM to investigate this relationship over the Sahara and
86 Sahel and reported little change in the dust emissions when moving from parameterized to explicit convection, but
87 also noted that the NLLJ maximum decreased as the convective maximum increased. Reinfried et al. (2009)
88 simulated a haboob case study from Morocco with the Lokal Modell - MultiScale chemistry aerosol transport (LM-
89 MUSCAT, since renamed COSMO-MUSCAT) regional model and found increased dust emissions in a convection-
90 allowing simulation versus those with cumulus parameterizations. They also established that the model was more
91 sensitive to the choice of cumulus parameterization rather than the change in horizontal resolution. Similarly, Bouet
92 et al. (2012) identified an increase in dust emissions with increasing model resolution using the Regional
93 Atmospheric Modeling System coupled to the Dust Prediction Model (RAMS-DPM) while simulating a Bodélé
94 depression case study. Ridley et al. (2013) showed that global aerosol models with parameterized convection were
95 also sensitive to model resolution and that higher horizontal resolution led to higher dust emissions.

96

97 With the added computational expense of running aerosol code, the resolution of dust forecast models lags relative
98 to their weather-only prediction counterparts for both global and regional prediction systems (Benedetti et al., 2014;
99 Benedetti et al., 2018). Efforts have been made to advance and evaluate predictive aerosol models and ensemble
100 aerosol modeling with working groups like the International Cooperative for Aerosol Prediction (ICAP) (Benedetti
101 et al., 2011; Reid, 2011; Sessions et al., 2015), and daily dust forecasts from several aerosol models are now
102 available through the World Meteorological Organization (WMO) Sand and Dust Storm Warning Advisory and
103 Assessment System (SDS-WAS) (http://www.wmo.int/sdswas). Nevertheless, none of the modeling groups in the

104 SDS-WAS currently run at fine enough grid-spacing to be considered convection-permitting (SDS-WAS Model
105 inter-comparison and forecast evaluation technical manual; last updated January, 2018). While regional numerical
106 weather prediction models have moved into convection-permitting scales, the added computational cost of aerosol
107 parameterizations means that convective parameterizations will be a necessity for longer in models that employ
108 online aerosol predictions. It is also clear that horizontal model resolution, be it specifically as to whether the grid-
109 spacing is fine enough to permit the explicit resolution of convective processes or is coarse enough to mandate
110 parameterized convection, is also still an understudied factor in regional dust modeling. As such, exploring
111 differences across cumulus parameterizations and those relative to convection-permitting resolutions remains
112 relevant and vital to better understand aerosol forecasting and aerosol-cloud-environment interactions.

113 While previous studies have begun to examine the effect of horizontal model resolution on dust emissions and
114 airborne dust concentrations, there are several factors that warrant more investigation. As it stands, there is little
115 agreement on the sign of the response in dust emissions to a change in model resolution, which seems to vary based
116 on the regional model being utilized. Most studies have concentrated on the change in dust emissions based on
117 moving from parameterized convection to convection-allowing scales, while ignoring the possible sensitivity due to
118 the choice of the cumulus parameterization itself. Furthermore, much of the previous literature focused on how the
119 increase in resolution affects convective outflow boundaries and surface / near-surface processes as dust sources,
120 rather than convective transport and the vertical redistribution of dust and its radiative effects at different levels of
121 the atmosphere. In this paper, we seek to address these limitations in the understanding of the effects of horizontal
122 model resolution on dust concentrations. The goal of the research presented here is therefore to quantify the sign and
123 magnitude in the response of modeled dust fields in a regional numerical model to increasing horizontal resolution.

124 In order to achieve our stated goal, we will use numerical simulations of a case study to examine the variability in
125 dust emissions and vertical dust concentrations and fluxes due to (1) the choice of convective parameterization, (2)
126 convection-allowing versus parameterized convection, and (3) the impact of these variations on radiation,
127 specifically aerosol heating rates. These simulations are performed using the Weather Research and Forecasting
128 Model coupled with Atmospheric Chemistry (WRF-Chem) (Skamarock et al., 2008; Grell et al., 2005; Fast et al.,
129 2006) a platform that has been tested for its sensitivity to vertical resolution for dust extinction coefficient profiles
130 (Teixeira et al., 2015) and horizontal model resolution and convective transport for chemical species such as carbon
131 monoxide (e.g. Klich and Fuelberg, 2013), but not for dust. These simulations will represent a case study of a
132 summertime coastal convective dust event over the Arabian Peninsula, a relatively understudied region compared to
133 areas such as the Sahara (Jish Prakash et al., 2015), despite being the world's second largest dust emission region
134 (Tanaka and Chiba, 2004).

135 This paper is part of a larger body of collaborative work conducted by the Holistic Analysis of Aerosols in Littoral
136 Environments (HAALE) research team under the Office of Naval Research Multidisciplinary Research Program of
137 the University Research Initiative (MURI). The primary goal of the HAALE-MURI project is to isolate the
138 fundamental environmental factors that govern the spatial distribution and optical properties of littoral zone aerosols.

139 The study discussed in this manuscript focuses on advancing our understanding in the role that convection plays in

140 the redistribution of dust aerosol and its radiative effects along the coast of arid regions, and seeks to quantify the

141 uncertainty in forecasted dust distributions stemming from the representation of convective processes in a regional

142 model.

143 The manuscript is organized as follows: an overview of the WRF-Chem model and physics setup (Sect. 2.1), dust

144 model setup (Sect. 2.2), information about the cumulus parameterizations and model resolution (Sect. 2.3), and

145 analysis methods in Sect. 2.4. A description of the case study is found in Sect. 2.5. The results are outlined in Sect.

146 3, with a discussion on the temporal evolution of dust concentrations and dust uplift potential in Sect. 3.1, vertical

147 distributions and fluxes of dust in Sect. 3.2, and the effect on aerosol radiative heating rates in Sect. 3.3. A

148 discussion of the results and implications for the community are located in Sect. 4 and a summary of the findings of

149 this study are reviewed in Sect. 5.

150 **2) Case study and model description**

151 **2.1) WRF-Chem model description and physics**

152 To investigate the Arabian Peninsula case study, WRF-Chem version 3.9.1.1 is used to simulate the dust outbreak

153 meteorology and aerosol fields. WRF-Chem is an online numerical chemical transport model that allows for

154 interactive aerosol processes, including feedbacks between the meteorology, aerosol, and radiation. The model is

155 coupled to the Goddard Chemistry Aerosol Radiation and Transport (GOCART) module (Ginoux et al., 2001),

156 which allows for feedbacks between the meteorology and aerosols and is described in more detail in Sect. 2.2.

157 The meteorological and sea surface temperature initial and lateral boundary conditions are sourced from the 0.25

158 degree, 6-hourly Global Data Assimilation System Final Analysis (GDAS-FNL). No chemistry or aerosol initial /

159 lateral boundary conditions are used. Rather, the aerosol fields are initialized with zero concentrations and are

160 allowed to evolve naturally from the model meteorology, aerosol, surface and radiation processes. The model is run

161 from 00:00:00 UTC on 02-Aug-2016 to 00:00:00 UTC on 05-Aug-2016 producing output at 30-minute intervals.

162 The following model parameterizations were employed and kept constant across the simulations, with similar WRF

163 physics options being utilized elsewhere to study dust effects (e.g. Alizadeh Choobari et al. 2013): Morrison double-

164 moment microphysics (Morrison et al., 2005; 2009), RRTMG longwave scheme (Iacano et al., 2008), Goddard

165 shortwave radiation scheme (Chou and Suarez, 1999), the Noah Land Surface Model with multiparameterization

166 options (Niu et al., 2011; Yang et al., 2011), and the MYNN level 3 boundary layer parameterization (Nakanishi and

167 Niino, 2006; 2009). The convective parameterizations and horizontal resolutions tested will be discussed in Sect.

168 2.4. A summary of the physics options utilized can be found in Table 1.

169 **2.2) GOCART dust emissions and dust uplift potential**

170 WRF-Chem is coupled to the GOCART dust module, which parameterizes the emission of dry mineral dust mass

171 from the surface to the atmosphere for 5 effective radii bins [0.5, 1.4, 2.4, 4.5, and 8.0 μm] based on Eq. (1):

172 $F_p = CSs_p U^2(U - U_t) \; if \; U > U_t$ (1)

173 In Eq. (1), F_p is the dust flux from the surface [kg m^{-2} s^{-1}] for each of the radii bins (p), S represents the wind erosion
174 scaling factor [0 to 1] established by the Ginoux et al. (2004) soil erodibility map, s_p is the fraction of each size class
175 within the soil [0 to 1] based on the silt and clay fraction of the soil type, U is the 10 m wind speed [m s^{-1}], and U_t is
176 the threshold velocity of wind erosion [m s^{-1}]. C is a tuning constant (set here to a default 1 kg s^2 m^{-5}), which can be
177 set by the user to increase or decrease the total dust flux based on regional observations (e.g. Zhao et al., 2010;
178 Kalenderski et al., 2013; Dipu et al., 2013). If the wind speed is less than the threshold velocity, no dust will loft
179 from the surface. Most of the terms in Eq. (1) are time invariant (C,S,s_p), except for the wind speed (U) and wind
180 erosion threshold (U_t). U_t is a function of soil wetness, and is calculated with the relationship found in Eq. (2):

181 $U_t = \begin{cases} 6.5\sqrt{\frac{\rho_p - \rho_a}{\rho_a} g D_p}(1.2 + log_{10}w_{soil}) & if \; w_{soil} < 0.5 \\ \infty & if \; w_{soil} \geq 0.5 \end{cases}$ (2)

182 For Eq. (2), ρ_p is the dust particle density [kg m^{-3}], ρ_a is the density of air [kg m^{-3}], g is gravitational acceleration [m
183 s^{-2}], and w_{soil} is the soil wetness fraction [0 to 1]. Similar to Eq. (1), Eq. (2) includes a threshold, whereby above a
184 soil wetness of 0.5, no dust will be emitted. If the threshold criteria are met and dust lofts from the surface, it is then
185 transported based on the simulated meteorological fields from WRF, including advection, convection, and turbulent
186 mixing, and is removed from the atmosphere via gravitational settling and wet deposition. Here, wet deposition is
187 included as a scavenging mechanism to provide a more realistic picture of the moist convection transport process.
188 Aerosol radiation interactions in the shortwave and longwave (Barnard et al., 2010) are included in the simulations
189 to understand the implications that lofted dust has on the energy budget of the case study and are discussed in Sect.
190 3.3.

191 Before dust can amass in and influence the atmosphere, it must first be emitted from the surface. Because of the
192 threshold values included in the GOCART dust parameterization equations (Eq. 1-2), it is important to understand
193 how often the modeled near-surface wind speeds exceed the wind threshold value. A parameter useful in describing
194 the influence of the wind on dust emissions is Dust Uplift Potential (DUP), proposed by Marsham et al. (2011) and
195 based on Marticorena and Bergametti (1995). The DUP parameter is an offline approximation for the relative
196 amount of dust expected to loft from the surface. DUP is a convenient way to perform first order sensitivity tests on
197 the meteorology without having to re-run the model, and provides a framework for deconvolving the variables in Eq.
198 (1-2). Here, we have adapted the DUP parameter from Marsham et al. (2011) (Eq. 4) into three variations (Eq. 3-5),
199 which allows researchers to vary the complexity of the analysis by including more, or fewer degrees of freedom.

200 $DUP(U) = U^3\left(1 + \frac{A}{U}\right)\left(1 - \frac{A^2}{U^2}\right)$ (3)

201 $DUP(U, U_t) = U^3\left(1 + \frac{U_t}{U}\right)\left(1 - \frac{U_t^2}{U^2}\right)$ (4)

202 $DUP(U, U_t, S) = SU^3\left(1 + \frac{U_t}{U}\right)\left(1 - \frac{U_t^2}{U^2}\right)$ (5)

203   In Eq. (3), U_t is set to a constant wind speed, A, thereby making DUP a function of only the near-surface wind

204   speed; for the purpose of this paper U_t is set to 5 m s^{-1}, but has been tested elsewhere across the range of 5-10 m s^{-1}

205   (e.g. Marsham et al., 2011; Cowie et al., 2015; Pantillon et al., 2015). This simplified equation for dust uplift has

206   been used in previous dust studies, and is useful to include here to place this manuscript in the context of existing

207   literature. Eq. (4) is slightly more intricate in that it considers the model evolution of U_t due to changing soil wetness

208   from precipitation and land-surface processes, calculated by Eq. (2). Lastly, Eq. (5) builds on Eq. (4) by including

209   the soil erodibility scaling factor (S), which recognizes that the U and U_t relationship is valid only if it occurs over

210   potential dust source regions. Since U, U_t, and S are entangled in the GOCART dust parametrization found in Eq.

211   (1-2), the seemingly minor variations between the DUP parameters in Eq. (3-5) are crucial for isolating which

212   processes, or combination of processes, are sensitive to the horizontal resolution of the model, and hence to the

213   analysis performed here.

214   **2.3) Domain, nesting, and cumulus parameterizations**

215   Several horizontal model grid-spacings (45 km, 15 km, and 3 km) of the Arabian Peninsula domain (Fig. 3) were

216   tested to identify the sensitivity of modeled dust concentrations to the model's horizontal resolution. For the two

217   coarsest simulations (45 km and 15 km), cumulus parameterizations were employed to represent shallow and deep

218   convection. The 45 km simulation was run with only the Betts–Miller–Janjic (BMJ) cumulus parameterization

219   (Janjic, 1994), while five different cumulus parameterizations were tested for the 15 km simulations, including the

220   BMJ, Kain–Fritsch (KF) (Kain, 2004), Grell 3D Ensemble (GD) (Grell, 1993; Grell et al., 2002), Tiedtke (TD)

221   (Tiedtke, 1989; Zhang et al., 2011), and Simplified Arakawa–Schubert (AS) (Arakawa and Schubert, 1974; Han and

222   Pan, 2011) schemes, which will determine the sensitivity of dust lofting to different cumulus parameterizations. A

223   15 km simulation with no cumulus parameterization was also run, but the results were similar and within the spread

224   of the 15 km simulations that employed cumulus parameterizations and are not included here. The finest resolution

225   simulation (3 km) was run at convection-permitting scales and hence no cumulus parameterizations were invoked.

226   The 3 km simulation was initialized as a one-way nest from the 15 km BMJ simulation which served as its parent

227   lateral boundary conditions. Other combinations of nests were tested, but the results were not sensitive to which 15

228   km simulation was used as the parent nest, or lateral boundary conditions, for the 3 km simulation. A summary of

229   the model domains is also found in Fig. 3.

230   The cumulus parameterizations tested in this study for the 15 km simulations vary in their methods for triggering

231   and then characterizing convective processes at the sub-grid scale level. BMJ is a moisture and temperature

232   adjustment scheme that acts to restore the pre-convective unstable thermodynamic profile to a post-convective stable

233   and well-mixed reference profile, while the other cumulus parameterizations (KF, GD, TD, AS) employ a mass-flux

234   approach to determine updraft and downdraft mass transport. Across the mass-flux parameterizations, GD is unique

235   in that it computes an ensemble of varying convective triggers and closure assumptions and then feeds the ensemble

236   mean back to the model. Furthermore, all five schemes represent shallow convection in addition to deep convection,

237   the mass-flux schemes include detrainment of water and ice at cloud top, and AS and TD are formulated to include

238   momentum transport in their calculations. These differences across parameterizations will result in varying updraft

239 and downdraft speeds and precipitation rates, which will have consequences for the vertical transport of airborne

240 dust, as well as the strength of convective outflow boundaries and therefore dust emission at the surface.

241 **2.4) Averaging and analysis methods**

242 Because the representation of convective processes varies across the simulations, the results will focus on composite

243 statistics from the three-day case study. The authors make no attempt to track and match individual convective

244 elements across simulations, as their triggering, timing, and development (or lack of development) will fluctuate

245 depending on the model resolution and cumulus parameterization, thus making a truly consistent analysis

246 problematic. Instead, this paper takes a step backward and aims to quantify in an average sense, how the choice of

247 horizontal resolution and parameterized convection affects dust concentrations in the WRF-Chem model across the

248 Arabian Peninsula. The analyses and averages are processed within the yellow box shown in Fig. 3, disregarding all

249 other grid points outside the Arabian Peninsula study area. Analyses that are averaged in time are only averaged

250 over the last two days of the simulation (00:00:00 UTC on 03-Aug-2016 to 00:00:00 UTC on 05-Aug-2016) to

251 account for model spin up in the first 24 hours. All results are summed over the five dust bins in the GOCART

252 model rather than being treated separately. Lastly, the results from the five 15 km simulations are averaged together

253 to produce a mean 15 km resolution response, and is presented, along with the maximum and minimum spread

254 across these simulations for reference.

255 **2.5) Case study overview**

256 The dust event simulated for this study occurred during August 2-5, 2016 across the Arabian Peninsula, originating

257 from a combination of synoptic and mesoscale dust sources. A meteorological analysis of this event, including an

258 attribution of specific dust sources to meteorological features can be found in Miller et al., 2019 and will not be

259 reiterated in detail here. Rather, a snapshot of the meteorology and dust fields from the WRF-Chem simulation on

260 August 3rd at 15:00:00 UTC can be found in Fig. 1-2 as a reference to the typical meteorological setup for this case

261 study.

262 For this event, the high summertime temperatures in the desert of the Arabian Peninsula produce a thermal low

263 couplet at the surface, with one low centered over Iraq and the other over the Rub' al Khali desert in Saudi Arabia

264 (Fig. 1.c). The local low-pressure couplet leads to cyclonic surface winds between these two areas (Fig. 1.e),

265 comprised of northerly flow from Iraq into Saudi Arabia, with retuning southerly flow from Oman over the Persian

266 Gulf and into Kuwait, and is a major non-convective contributor to the dust budget for this case study (Fig. 1.f). In

267 addition to these large-scale flow patterns, a daytime sea breeze brings moist, maritime air from the coast of Yemen

268 and Oman inland into the otherwise arid Saudi Arabian basin (Fig. 1.e and 1.d). This moisture gradient is also

269 evident in the skew-t diagrams, which represent an inland radiosonde release site at Riyadh (Fig. 2.a), and a site

270 closer to the coast in Abha (Fig. 2.b), both located in Saudi Arabia. There is a stark difference in low-level moisture

271 between the two sites, although both display a subsidence inversion aloft between 500 and 600 hPa. Furthermore,

272 nocturnal low-level jets form along the Zagros mountains in Iran and Iraq, and the Red sea, both of which have been

273 studied previously in the literature (Giannakopoulou and Toumi, 2011; Kalenderski and Stenchikov, 2016).

274 Due to the region's inherent moisture constraints, convection is limited spatially to the coastal regions of the
275 Arabian Peninsula, as is most summertime convective and non-convective precipitation in this region (e.g. Shwehdi,
276 2005; Almazroui, 2011; Hasanean and Almazroui, 2015; Babu et al., 2016). Moist convective cells develop along a
277 low-level convergence line between the northerly basin flow and sea breeze front (Fig. 1.g and 1.h) aided by
278 elevated terrain in Yemen and Oman (Fig. 1.a). This convective setup along the southern portion of the Arabian
279 Peninsula is a feature evident in each day of this case study, initializing diurnally in the local late afternoon and early
280 evening, and thereby providing three days of data for analysis, with the height of convective activity occurring on
281 August 3rd. Individual convective cells form along the convergence line, a typical Middle Eastern characteristic
282 (Dayan et al., 2001), but do not organize further, owing to a lack of upper-level synoptic support and insufficient
283 moisture in the interior of the peninsula. Nevertheless, the convective line does produce outflow boundaries, which
284 loft dust from the surface and are the main convective dust source for this case study. More information on the
285 meteorological setup of this case study, including comparisons with aerosol optical depth (AOD) observations can
286 be found in Saleeby et al. (2019).

287 **3) Results**

288 **3.1) Temporal evolution**

289 **3.1.1) Dust uplift potential**

290 The first process of interest in determining the sensitivity of modeled dust concentrations to horizontal resolution in
291 WRF-Chem is the amount of dust lofted from the surface to the atmosphere. Fig. 4 depicts the average DUP for the
292 simulations at each 30-minute output, using Eq. (3-5) to separate out the importance of the different mechanisms
293 regulating dust emissions.

294 Regardless of which DUP parameter is used, almost all of the simulations capture the bimodal daily maximum in
295 dust emissions in the local mid-morning (6 UTC) and late afternoon (13 UTC) due to the mixing of the NLLJ to the
296 surface and convective outflow boundaries, respectively. The only resolution where the bimodality is absent is the
297 45 km simulation, which captures the NLLJ mechanism, but misses the second convective activity maximum. The
298 coarsest simulation overestimates the near-surface wind speeds related to the NLLJ mechanism, which subsequently
299 inhibits convection later in the day. Because of this, the 45 km simulation has the highest DUP(U) (Fig. 4.a) based
300 only on wind speed (Eq. 3), a result similar to the Heinhold et al. (2013) and Marsham et al. (2011) studies over the
301 Sahara.

302 However, when taking the calculated threshold wind velocity into account (Eq. 4), the convection-allowing
303 simulation (3 km) displays the strongest DUP(U,U_t) at the local late afternoon convective maximum (Fig. 4.c). For
304 this to be the case compared to the DUP(U) parameter, the 3 km simulation must have a lower threshold wind
305 velocity (Fig. 5.a) than the simulations with parameterized convection. Since the threshold wind velocity is
306 proportional to soil wetness (Eq. 2), this implies that the convection-permitting simulation will on average have drier

307   soil, or more grid points below the soil wetness threshold than the parameterized simulations. Rainfall is generated

308   differently in parameterized versus convection-allowing simulations, and it has been well documented that

309   parameterized simulations produce more widespread light rainfall, whereas more intense rainfall tends to develop

310   over smaller areas in convection-allowing simulations (e.g. Sun et al., 2006; Stephens et al., 2010). From a domain

311   average perspective, rainfall in the 3 km simulation will cover less area, leading to the soil moisture threshold not

312   being exceeded as frequently compared to the parameterized cases.

313   This spatial difference in rainfall leads to the 3 km case having drier soil on average across the domain, which is

314   evident in the surface fluxes represented by the Bowen ratio of sensible to latent heat fluxes in Fig. 5.c. When the

315   Bowen ratio is above one, more of the surface heat exchange with the atmosphere is in the form of sensible heat

316   flux, rather than latent heat flux. Dry soils are characterized by low values of latent heat flux, and therefore exhibit

317   higher Bowen ratios. The 3 km simulation exhibits a higher Bowen ratio on August 3rd and 4th, indicating that the

318   soil is on average drier in the convection-permitting simulation. This result implies that disparities in land surface

319   properties across the varying model grid resolutions are important for modulating dust emissions, both from the

320   perspective of convection-allowing versus parameterized convection and associated precipitation, as well as latent

321   and sensible heat fluxes.

322   Adding on to the complexity of the DUP parameter, when the location of dust sources is considered in the

323   DUP(U,U_t,S) calculations (Eq. 5), some of variability between the local NLLJ and convection maxima is lost in the

324   3 km simulation (Fig. 4.e) on August 3rd. Also, including the scaling factor reduces the magnitude of the DUP

325   parameter to roughly 10% of the initial values for DUP(U) and DUP(U,U_t). Incorporating the dust source function in

326   DUP works not only as a scaling factor for the magnitude of potential dust emissions, but also impacts the relative

327   importance of dust production mechanisms (NLLJ versus convection). This shift is a consequence of the location in

328   which these processes occur. For instance, the reduction in the 3 km convective maximum on August 3rd between

329   DUP(U,U_t) and DUP(U,U_t,S) signifies that convection is occurring in locations that are not active dust source

330   regions. Without information on the dust source regions, this process would be assigned an unrealistic dominance

331   over the NLLJ mechanism in terms of DUP.

332   All simulations are similar for the first 24 spin-up hours until the processes begin to diverge on August 3rd, where

333   the convection-allowing simulation produces the maximum DUP(U,U_t,S) both during the local daytime and

334   nighttime hours. On the final day of the case study (August 4th), the convection-allowing simulation has the lowest

335   DUP(U,U_t,S), with the NLLJ maximum dominating over the convective maximum in both the 3 km and the 15 km

336   mean, due to reduced convective activity in the fine resolution simulations. Examining the percent difference in

337   DUP between the coarse and fine simulations (Fig. 4.b,d,f), the average percent difference between the 3 km and 15

338   km simulations is at a minimum when only wind speed is considered, and increases as the degrees of freedom in

339   DUP increases. For the DUP(U,U_t,S) case, the average percent difference is between 10-65% lower in the 15 km

340   simulations than the convection-permitting simulation, with a maximum difference of 85% and a spread across

341   parameterizations of 20%. This implies that the convection-allowing WRF-Chem simulation has the potential to loft

342   up to 85% more dust than those with parameterized convection.

343   **3.1.2) Vertically integrated dust mass**

344   The differences in DUP(U,U_t,S), or dust flux from the surface to the atmosphere, specifically the enhanced values

345   for the convection-permitting simulation on August 3rd, will lead to more dust lofting than in the coarse simulations.

346   To see how differences in the dust emissions translate into differences in airborne concentrations of dust, Fig. 6

347   demonstrates the temporal evolution of the spatially averaged, vertically integrated dust mass throughout the vertical

348   column. Here, the convection-allowing simulation records upwards of 150% more integrated dust mass compared to

349   the coarse resolution simulations. Across the coarse simulations, the 45 km and 15 km runs have similar vertically

350   integrated dust magnitudes, despite the temporal differences in DUP(U,U_t,S). This is due to the overestimation of

351   the NLLJ in the 45 km simulations being offset by the enhanced convective dust lofting in the 15 km simulations.

352   The discrepancy in the diurnal maxima across horizontal resolutions is similar to the results of the UM in Marsham

353   et al. (2011) and Heinhold et al. (2013). Yet, the results here differ in that both of these previous studies found a

354   stronger NLLJ response in 12 km simulations with convective parameterizations than was found here in the 15 km

355   parameterized ensemble. In contrast to the findings of Marsham et al. (2011) and Heinhold et al. (2013), dust

356   emissions and airborne dust mass increases in the WRF-Chem simulations in the convection-allowing simulation,

357   which is in closer agreement to the studies of Reinfried et al. (2009) and Bouet et al. (2012) who used COSMO-

358   MUSCAT and RAMS-DPM respectively. Considering each study used a different model and therefore physics, it is

359   unsurprising that the results vary. However, it is not apparent how much of a role the region or specific case study

360   plays in this difference and is an area for future work.

361   The temporal trends in vertically integrated dust mass lag behind those observed in the DUP plots in Fig. 4.

362   Particularly at timesteps where DUP decreases, the change in integrated dust mass follows several hours later. The

363   time series of gravitational settling rates at the surface (Fig. 5.b) also lags behind the DUP trends, which implies that

364   the removal mechanisms for dust take time to act on the airborne particles once they are emitted. The rates of

365   gravitational settling are higher in the convection-permitting simulation compared to the coarse simulations because

366   more dust is available aloft to settle out. Nevertheless, Fig. 6.a suggests that this increase in gravitational settling

367   rates in the 3 km case is not enough to offset the higher dust emissions, or the vertically integrated dust quantities

368   would be similar across all the simulations. The fact that the vertically integrated dust values are higher in the 3 km

369   simulation, despite higher rates of gravitational settling, implies there must be a mechanism that acts to keep dust

370   suspended longer in the convection-permitting simulations than in those with parameterized convection. There are

371   clearly more processes occurring above the surface to influence the vertically integrated dust quantities than just a

372   simple surface emission to surface deposition ratio. This will be further deconstructed by examining vertical profiles

373   in the following section.

374 **3.2) Vertical characteristics**

375 **3.2.1) Vertical dust and velocity profiles**

376 Moving away from vertically integrated quantities to a time and domain averaged vertical snapshot of dust (Fig.

377 7.a), the vertical dust profile follows a generally exponentially decreasing function and tapers off to low dust

378 concentrations in the range of 5-6 km above ground level (AGL). A widespread subsidence inversion is present near

379 6 km throughout the case study time period over the inner basin of the Arabian Peninsula (Fig 2), acting as a cap on

380 vertical motions and dust transport. Because dust concentrations do not vary much above this height, the plots in

381 Fig. 7 have been truncated at 9 km. There is a higher concentration of dust at every level in the convection-allowing

382 simulation compared to that in the coarse simulations. Examining the percent difference plot between the

383 convection-permitting and other simulations in Fig. 7.b, there is a difference of approximately 80% at the surface,

384 which increases upwards to ~180% at 6 km. Above this level, the percent difference between the convection-

385 permitting and coarse simulations changes sign, but the overall concentration is extremely low, and as such, the

386 authors make no attempt to assign meaning to the differences above 6 km.

387 For dust to reach higher levels in the atmosphere, it must have undergone vertical transport to move it aloft from its

388 initial source region at the surface. Several mechanisms could be responsible for vertical dust transport in the

389 Arabian Peninsula, including flow over terrain, daytime mixing (dry convection), and lastly, moist convective

390 updrafts, whose representation (explicit versus parameterized) is a defining difference between the horizontal

391 resolutions tested in this paper. Investigating the effect that increasing resolution has on updraft and downdraft

392 strength can be found in Fig. 8, which represents the mean of all vertical velocities above or below 0 m s^{-1}, including

393 points that are not vertically continuous. As resolution increases, the average range in vertical velocity also

394 increases. The simulations with parametrized convection have lower mean updraft / downdraft speeds than the

395 convection-allowing simulation, on the order ~75% weaker near the surface for the 15 km runs and ~110% weaker

396 for the 45 km run. It is known that in numerical models, the updraft radius scales with the grid spacing (e.g. Bryan

397 and Morrison, 2012), with a compensating increase in updraft speed as the radius decreases. This relationship skews

398 the frequency of vertical velocities to higher values. Irrespective of resolution, the mean updraft speeds in the WRF-

399 Chem simulations are slightly higher than the downdraft speeds, while at the surface mean downdraft speeds are

400 higher than updraft speeds, a consideration that will be discussed further in Sect. 3.2.2.

401 **3.2.2) Vertical dust flux**

402 The implication for dust transport based on vertical velocities is convoluted, since updrafts and downdrafts work

403 concurrently to redistribute aerosol. As noted in Jung et al. (2005), convective updrafts will lift aerosol particles

404 upward into the free atmosphere, while downdrafts simultaneously limit the maximum vertical extent of these

405 particles. However, the convective transport simulations in Jung et al. (2005) demonstrate that these opposing

406 processes do not act as equal opposites in time, magnitude, and space. This canon holds true for the Arabian

407 Peninsula simulations as well. Fig. 9 contains Contoured Frequency by Altitude Diagrams (CFADs) of vertical

408 velocity (Yuter and Houze, 1995) normalized by the total number of grid points in each simulation. The

409   normalization is performed to remove an artificial larger frequency in the higher resolution simulations that arises

410   because there are more grid spaces available to count. Because no vertical velocity threshold is imposed, a majority

411   of points straddle zero. To highlight variability away from the zero line, the CFAD contours are plotted on a log

412   scale.

413   Similar to the mean plots in Fig. 8, as resolution increases, so does the variability in updraft and downdraft speeds.

414   There is a striking difference between the spread in vertical velocities at all altitudes across the 45 km, 15 km mean,

415   and 3 km simulations in Fig. 9. In the 45 km run, most of the velocities straddle +/- 1-2 m s^{-1}, whereas the

416   convection-permitting simulation ranges from -10 to 30 m s^{-1}. Not only is the range larger, but the normalized

417   frequency is greater in the fine resolution simulation as well. The inference here is that stronger updrafts will

418   transport dust higher in the atmosphere, and that stronger updrafts are observed more frequently in the convection-

419   allowing simulation, thereby enhancing the vertical dust transport.

420   Combining the information on the vertical distribution of dust and updraft / downdraft speeds, it is possible to

421   calculate a domain averaged dust flux profile (Fig. 8). Again, the magnitude of the dust flux upwards and

422   downwards from the surface through 6 km AGL is higher in the convection-allowing simulation compared to the

423   parametrized simulations. Moreover, the mean near-surface upwards dust flux is stronger than that for the downward

424   dust flux, which coincides with the mean updraft speeds being slightly higher than the mean downdraft speeds at

425   these same vertical levels (Fig. 8). This relationship also holds in the dust flux CFADs (Fig. 9), in which the upward

426   and downward flux of dust has more variability in the 3 km simulation, and stronger vertical dust fluxes are more

427   frequent.

428   Similarly, there is more dust transport evident at higher vertical levels in the convection-permitting simulation,

429   which has implications for the residence time of the dust particles. As dust is transported higher in the atmosphere,

430   absent any sort of external motion or coagulation outside of gravitational settling, the atmospheric lifetime of the

431   particles will increase. Figure 10 shows the theoretical terminal velocity of dust particles in WRF-Chem using the

432   Stokes settling velocity with slip correction for pressure dependence (Fig. 10.a) and their lifetime based on different

433   starting heights in the atmosphere (Fig. 10.b), which increases exponentially away from the surface. As such, dust in

434   the convection-permitting simulation will take longer to settle out, leading to the higher observed vertically

435   integrated dust values (Fig. 5) compared to the parameterized simulations. Looking at the distribution of downdrafts

436   in the vertical velocity CFADs (Fig. 9), there is a clear bimodal signal aloft in both the convection-permitting and 15

437   km simulations, being representative of two distinct subsidence layers, which act as a cap on vertical transport. The

438   local minimum occurs around 6 km, which could explain why dust fluxes also taper off at this level.

439   At the surface, higher dust flux values are found in association with the downdrafts, producing a pronounced

440   skewness towards high, yet infrequent values of strong negative dust flux towards the ground (Fig. 9). It is

441   hypothesized that this skewness is a consequence of the dissimilar background dust conditions in the vicinity of

442   near-surface downdrafts and updrafts, similar to the results found in Siegel and van den Heever (2012), which

443   studied the ingestion of dust by a supercell storm. Updrafts originate in relatively clear air, and will consume

444 background dust and transport it upwards. However, downdrafts occur through the cold pool, and hence their source

445 is, at least partially, within the dusty cold pool. As such, downdrafts will have access to more dust and thus transport

446 more of it in the downward direction. This skewness warrants further research, preferably from an idealized

447 perspective, to better understand the relationship between storm dynamics, dust emissions, and transport.

448 In all, the increased vertical dust concentration profile and vertically integrated dust values in the 3 km run are a

449 product of several processes working together. Compared to the simulations with parameterized convection, the 3

450 km run has enhanced potential for dust uplift due to stronger resolved downdrafts and lower wind velocity

451 thresholds, higher vertical transport due to more frequent, stronger updrafts, and a lengthier theoretical residence

452 time once being lofted to higher levels.

453 **3.3) Impacts on radiation**

454 Beyond the first-order sensitivity of model resolution to dust emissions and concentrations for the Arabian Peninsula

455 case study, there are higher-order effects that disseminate from changing dust concentrations. One example being

456 the modification of atmospheric heating / cooling rates and the radiation budget due to dust absorption and scattering

457 (see Sect. 1). The domain and time averaged shortwave (SW), longwave (LW), and net dust heating / cooling rates

458 are found in Fig. 11. The average dust heating and cooling rates were calculated over the last 48 hours of the

459 simulation as a difference between the radiation tendency with dust aerosols and without. Ostensibly, since dust

460 concentrations increase in the model as resolution increases, so does the magnitude of the radiative effects. There is

461 a stronger SW cooling and LW heating effect in the 3 km simulation, and this trend follows the vertical distribution

462 of dust from Fig. 7, again tapering off near 5-6 km AGL.

463 Most interestingly, however, is the difference in the net aerosol heating rate. In the lowest layer (<1.5 km), there is a

464 sign change between the fine and coarse simulations. The SW effect in the convection-allowing simulation is strong

465 enough to elicit a net cooling effect in this near-surface layer. Conversely, the LW aerosol heating effect dominates

466 in the coarse simulations, resulting in a net warming effect. The model has a stronger shortwave effect for dust based

467 on the prescribed index of refraction, but is also related to the timing of dust emissions, considering the SW effect is

468 only active during the daytime. The difference between warming and cooling can have cascading effects on the

469 thermodynamic profile, static stability, and future convective development, which in turn impacts the relative

470 importance between convection and the NLLJ discussed earlier. The sensitivity of dust concentrations to horizontal

471 model resolution is important to understand in its own right, but furthermore, this sensitivity leads to higher-order

472 changes in model predictions. If NWP models or GCMs are going to incorporate dust radiative effects,

473 concentrations need to be highly constrained, not only to accurately capture the magnitude, but the sign of the

474 response as well.

475 **4) Discussion and recommendations**

476   For this Arabian Peninsula event, horizontal resolution in the WRF-Chem model has a considerable effect on the

477   dust budget of the region. Because aerosol prediction models and GCMs still employ cumulus parameterizations, it

478   is important to discuss the uncertainties unearthed in this paper, as well as recommendations for past and future

479   forecasts and research that will be generated prior to our ability to consistently run these models at convection-

480   permitting resolutions.

481   In an average sense, there will be higher dust concentrations produced in convection-permitting simulations

482   compared to those with parameterized convection. The major point here is that the uncertainty in dust concentrations

483   for simulations using different cumulus parameterizations (15 km ensemble), or using different horizontal

484   resolutions with the same cumulus parameterizations (45 km versus 15 km) is small relative to the differences

485   between the use of parameterized versus convection-allowing scales. *Most of the uncertainty in the model's*

486   *predicted dust concentrations comes from the choice to either parameterize convection or run at convection-*

487   *permitting scales.*

488   The results of this research do not stand alone in the literature focused on the impact of horizontal model resolution

489   on dust emissions, and there are several similarities and differences to note when comparing this paper to previous

490   studies. Firstly, concerning the diurnal variation in dust emissions, we find a similar response in the NLLJ

491   mechanism to that of Heinhold et al. (2013) and Marsham et al. (2011), whereby the coarsest simulations

492   overestimate the early morning windspeeds caused by the mixing of the jet to the surface and fail to capture the late

493   afternoon / early evening convective dust lofting mechanism. In these previous studies, the convection-allowing

494   simulation reduces the importance of the NLLJ and enhances the convective maximum, but still retains the NLLJ as

495   the dominant process for dust uplift. Overall, Heinhold et al. (2013) and Marsham et al. (2011) found a net reduction

496   in dust uplift while running at convection-permitting scales. While the NLLJ mechanism is found to be similar here,

497   the analysis reveals an opposite response in WRF-Chem for the Arabian Peninsula, in which the convective

498   maximum dominates, but the NLLJ is still an important mechanism, which thereby leads to more, rather than less

499   dust in the convection-allowing simulations. The net increase in dust concentrations in WRF-Chem is similar to the

500   findings of Reinfried et al. (2009), although Reinfried et al. (2009) focused mainly on haboobs, which may point to

501   convection being the source of agreement rather than the balance between the NLLJ and convection. At this point,

502   we cannot determine whether the discrepancies between our results and previous literature comes from regional or

503   case study differences in the importance of these mechanisms to the dust budget, differences in the models'

504   representation of these processes, or a combination of the two. In all, more work needs to be done to investigate the

505   relationship between the NLLJ and subsequent late afternoon convection in dust producing regions, and the

506   representation of this in numerical models.

507   From a vertically integrated viewpoint, for the Arabian Peninsula region it is possible to rudimentarily tune the dust

508   concentrations of the coarse simulations to that of the convection-permitting simulation by multiplying by an

509   average constant derived from the dust difference plots in Fig. 6-7, which would be on the order of ~2. This is an

510   offline solution, which would aid in enhancing the accuracy of a first-order forecast of vertically integrated or

511 surface dust, and/or AOD. Nevertheless, attempting to use this tuning parameter online in the model (i.e. adjusting

512 the tuning constant, C, in Eq. 1) would not reconcile the differences from a dust flux standpoint. Even if more dust

513 were to be emitted from the surface, the parameterized simulations still lack the necessary variability in updrafts and

514 downdrafts, especially updraft strength, to transport the dust upwards and away from the surface, thus

515 misrepresenting the atmospheric lifetime of these particles in the process.

516 Moreover, tuning the dust concentrations will not change the effect horizontal resolution has on the soil

517 characteristics, particularly soil moisture, and hence on the a priori determined threshold wind speeds which are

518 important in calculating dust lofting in the first place (Fig. 4). If dust concentrations are inaccurately predicted in the

519 coarse simulations, or erroneously tuned, the higher-order online feedbacks will also be incorrect, such as

520 modifications to the radiative budget, and feedbacks to the thermodynamic profile, static stability and mesoscale

521 features, particularly those driven by differences in thermodynamic gradients, such as sea breezes and cold pool

522 propagation.

523 **5) Conclusions**

524 In this study, we have quantified the response sign and magnitude in modeled dust fields in the WRF-Chem regional

525 model to increasing horizontal resolution and the manner in which convection is represented for a summertime

526 Arabian Peninsula event. We have investigated the variability in dust concentrations and fluxes due to the choice of

527 convective parameterization, the representation of convection in the model (explicit versus parameterized), and the

528 effect these differences in dust concentrations have on aerosol heating rates. The case study was simulated at three

529 different horizontal resolutions (45 km, 15 km, and 3 km), with the two coarsest simulations run with cumulus

530 parameterizations, and the 3 km simulation run at convection-permitting resolution. To understand the uncertainty

531 across different parameterizations, five separate cumulus parameterizations were tested in an ensemble (BMJ, AS,

532 GD, TD, KF) at 15 km grid spacing.

533 The convection-allowing simulation exhibited a stronger potential for dust uplift as a function of modeled wind

534 speed, wind threshold, and the location of dust sources. The wind threshold for dust lofting in the 3 km simulation

535 was on average, lower than that for the 15 km or 45 km. This is due to differences in grid resolution leading to

536 changes in the soil moisture, whereby the 3 km simulation displays lower soil wetness across the domain.

537 Furthermore, a distinct difference across simulations was identified in the representation of the bimodal daily

538 maximum in dust emissions in the local mid-morning (mixing of the NLLJ to the surface) and late afternoon

539 (convective outflow boundaries). Compared to the 3 km case, the 45 km simulation overestimates the contribution

540 from the NLLJ and underestimates the role of convection in dust emissions.

541 The 3 km simulation also produced higher vertically integrated dust values at every timestep, as well as higher dust

542 concentrations at every vertical level in the lower troposphere (below 6 km AGL). The uncertainty in dust

543 concentrations for simulations using different cumulus parameterizations (15 km ensemble spread) is much smaller

544 than the difference between the parameterized and convection-permitting convection cases. For the WRF-Chem

545 Arabian Peninsula simulations, the modeled dust fields were most sensitive to the choice of parametrizing or
546 explicitly resolving convective processes. The enhanced dust concentrations in the convection-allowing case are the
547 result of stronger downdrafts lofting more dust from the surface, and stronger updrafts carrying dust to higher levels
548 of the atmosphere, thereby increasing the airborne lifetime of the dust particles. The difference in dust mass across
549 the simulations leads to a significant modification of the radiation budget, specifically the aerosol heating rate. The
550 convection-allowing simulation revealed a greater shortwave and longwave effect, and for aerosol heating rates in
551 the lowest levels, shortwave cooling is stronger than longwave heating, leading to a net cooling effect. Conversely,
552 the opposite radiative response is present in the parameterized cases, resulting in a net warming effect, causing a
553 change in sign in the lowest levels compared to the convection-permitting case.

554 There are a number of implications these results may have on forecasting and future studies. The dust concentrations
555 in the coarse simulations could be tuned offline to match those in the convection-allowing simulation using the
556 percentage difference plots included in Fig. 5-6. This tuning would be on the order of ~2. However, because vertical
557 transport is essential to the vertical concentrations and lifetime of the particles, this tuning factor cannot be applied
558 online. Even if such a tuning were applied, this change will not accurately capture higher-order feedbacks to the
559 meteorology, thermodynamic environment and radiation budget of the Arabian Peninsula, or to the soil moisture
560 wind threshold velocities. Finally, this work also points to the need to better constrain dust concentrations in
561 numerical models, and further develop our understanding of the relationship between storm dynamics and dust
562 processes.

563 **Author contributions**

564 Jennie Bukowski (JB) and Susan C. van den Heever (SvdH) designed the experiments. JB set up and performed the
565 WRF-Chem simulations and wrote the analysis code. Both JB and SvdH contributed to the analysis of the model
566 output. JB prepared the manuscript with contributions and edits from SvdH.

567 **Competing interests**

568 The authors declare that they have no conflict of interest.

569 **Acknowledgements**

570 This work was funded by an Office of Naval Research – Multidisciplinary University Research Initiative (ONR-
571 MURI) grant (# N00014-16-1-2040). Jennie Bukowski was partially supported by the Cooperative Institute for
572 Research in the Atmosphere (CIRA) Program of Research and Scholarly Excellence (PRSE) fellowship. The
573 simulation data are available upon request from the corresponding author, Jennie Bukowski. Initialization data for
574 the model was provided by: National Centers for Environmental Prediction, National Weather Service, NOAA, U.S.
575 Department of Commerce. 2000, updated daily. NCEP FNL Operational Model Global Tropospheric Analyses,

576 continuing from July 1999. Research Data Archive at the National Center for Atmospheric Research, Computational
577 and Informational Systems Laboratory. https://doi.org/10.5065/D6M043C6.

578 **References**

579 Alizadeh Choobari, O., Zawar-Reza, P., and Sturman, A.: Low level jet intensification by mineral dust aerosols,
580   Ann. Geophys., 31, 625–632, doi:10.5194/angeo-31-625-2013, 2013.

581 Almazroui, M.: Calibration of TRMM rainfall climatology over Saudi Arabia during 1998–2009, Atmos. Res.,
582   99(3–4), 400–414, doi:10.1016/J.ATMOSRES.2010.11.006, 2011.

583 Aoki, T., Tanaka, T. Y., Uchiyama, A., Chiba, M., Mikami, M., Yabuki, S. And Key, J. R.: Sensitivity Experiments
584   of Direct Radiative Forcing Caused by Mineral Dust Simulated with a Chemical Transport Model, J.
585   Meteorol. Soc. Japan. Ser. II, 83A, 315–331, doi:10.2151/jmsj.83A.315, 2005.

586 Arakawa, A. and Schubert, W. H.: Interaction of a Cumulus Cloud Ensemble with the Large-Scale Environment,
587   Part I, J. Atmos. Sci., 31(3), 674–701, doi:10.1175/1520-0469(1974)031<0674:IOACCE>2.0.CO;2, 1974.

588 Babu, C. A., Jayakrishnan, P. R. and Varikoden, H.: Characteristics of precipitation pattern in the Arabian Peninsula
589   and its variability associated with ENSO, Arab. J. Geosci., 9(3), 186, doi:10.1007/s12517-015-2265-x,
590   2016.

591 Baddock, M. C., Strong, C. L., Leys, J. F., Heidenreich, S. K., Tews, E. K. and McTainsh, G. H.: A visibility and
592   total suspended dust relationship, Atmos. Environ., 89, 329–336, doi:10.1016/J.ATMOSENV.2014.02.038,
593   2014.

594 Barnard, J. C., Fast, J. D., Paredes-Miranda, G., Arnott, W. P. and Laskin, A.: Technical Note: Evaluation of the
595   WRF-Chem "Aerosol Chemical to Aerosol Optical Properties Module" using data from the MILAGRO
596   campaign, Atmos. Chem. Phys., 10(15), 7325–7340, doi:10.5194/acp-10-7325-2010, 2010.

597 Beegum, S. N., Gherboudj, I., Chaouch, N., Temimi, M. and Ghedira, H.: Simulation and analysis of synoptic scale
598   dust storms over the Arabian Peninsula, Atmos. Res., 199, 62–81, doi:10.1016/J.ATMOSRES.2017.09.003,
599   2018.

600 Benedetti, A., Reid, J. S., Knippertz, P., Marsham, J. H., Di Giuseppe, F., Rémy, S., Basart, S., Boucher, O., Brooks,
601   I. M., Menut, L., Mona, L., Laj, P., Pappalardo, G., Wiedensohler, A., Baklanov, A., Brooks, M., Colarco,
602   P. R., Cuevas, E., da Silva, A., Escribano, J., Flemming, J., Huneeus, N., Jorba, O., Kazadzis, S., Kinne, S.,
603   Popp, T., Quinn, P. K., Sekiyama, T. T., Tanaka, T. and Terradellas, E.: Status and future of numerical
604   atmospheric aerosol prediction with a focus on data requirements, Atmos. Chem. Phys., 18(14), 10615–
605   10643, doi:10.5194/acp-18-10615-2018, 2018.

606 Benedetti, A., Baldasano, J. M., Basart, S., Benincasa, F., Boucher, O., Brooks, M. E., Chen, J.-P., Colarco, P. R.,
607   Gong, S., Huneeus, N., Jones, L., Lu, S., Menut, L., Morcrette, J.-J., Mulcahy, J., Nickovic, S., Pérez
608   García-Pando, C., Reid, J. S., Sekiyama, T. T., Tanaka, T. Y., Terradellas, E., Westphal, D. L., Zhang, X.-
609   Y. and Zhou, C.-H.: Operational Dust Prediction, in Mineral Dust: A Key Player in the Earth System,
610   edited by P. Knippertz and J.-B. W. Stuut, pp. 223–265, Springer Netherlands, Dordrecht., 2014.

611 Benedetti, A., Reid, J. S. and Colarco, P. R.: International Cooperative for Aerosol Prediction Workshop on Aerosol

612   Forecast Verification, Bull. Am. Meteorol. Soc., 92(11), ES48-ES53, doi:10.1175/BAMS-D-11-00105.1,

613   2011.

614   Bishop, J. K. B., Davis, R. E. and Sherman, J. T.: Robotic Observations of Dust Storm Enhancement of Carbon

615   Biomass in the North Pacific, Science (80-.)., 298(5594), 817 LP-821, doi:10.1126/science.1074961, 2002.

616   Boose, Y., Welti, A., Atkinson, J., Ramelli, F., Danielczok, A., Bingemer, H. G., Plötze, M., Sierau, B., Kanji, Z. A.

617   and Lohmann, U.: Heterogeneous ice nucleation on dust particles sourced from nine~deserts worldwide --

618   Part 1: Immersion freezing, Atmos. Chem. Phys., 16(23), 15075–15095, doi:10.5194/acp-16-15075-2016,

619   2016.

620   Bouet, C., Cautenet, G., Bergametti, G., Marticorena, B., Todd, M. C. and Washington, R.: Sensitivity of desert dust

621   emissions to model horizontal grid spacing during the Bodélé Dust Experiment 2005, Atmos. Environ., 50,

622   377–380, doi:10.1016/J.ATMOSENV.2011.12.037, 2012.

623   Bryan, G. H., and Morrison, H.: Sensitivity of a Simulated Squall Line to Horizontal Resolution and

624   Parameterization of Microphysics, MWR, 140, 202-225, doi:10.1175/MWR-D-11-00046.1, 2012.

625   Camino, C., Cuevas, E., Basart, S., Alonso-Pérez, S., Baldasano, J. M., Terradellas, E., Marticorena, B., Rodríguez,

626   S. and Berjón, A.: An empirical equation to estimate mineral dust concentrations from visibility

627   observations in Northern Africa, Aeolian Res., 16, 55–68, doi:10.1016/J.AEOLIA.2014.11.002, 2015.

628   Chou, M.-D. and Suarez, M. J.: Technical Report Series on Global Modeling and Data Assimilation A Thermal

629   Infrared Radiation Parameterization for Atmospheric Studies Revised May 2003, Nasa Tech. Memo. 15,

630   NASA, 40 pp., 1999.

631   Corr, C. A., Ziemba, L. D., Scheuer, E., Anderson, B. E., Beyersdorf, A. J., Chen, G., Crosbie, E., Moore, R. H.,

632   Shook, M., Thornhill, K. L., Winstead, E., Lawson, R. P., Barth, M. C., Schroeder, J. R., Blake, D. R. and

633   Dibb, J. E.: Observational evidence for the convective transport of dust over the Central United States, J.

634   Geophys. Res. Atmos., 121(3), 1306–1319, doi:10.1002/2015JD023789, 2016.

635   Cowie, S. M., Marsham, J. H. and Knippertz, P.: The importance of rare, high-wind events for dust uplift in northern

636   Africa, Geophys. Res. Lett., 42(19), 8208–8215, doi:10.1002/2015GL065819, 2015.

637   Dayan, U., Ziv, B., Margalit, A., Morin, E. and Sharon, D.: A severe autumn storm over the middle-east: synoptic

638   and mesoscale convection analysis, Theor. Appl. Climatol., 69(1), 103–122, doi:10.1007/s007040170038,

639   2001.

640   Dipu, S., Prabha, T. V., Pandithurai, G., Dudhia, J., Pfister, G., Rajesh, K. and Goswami, B. N.: Impact of elevated

641   aerosol layer on the cloud macrophysical properties prior to monsoon onset, Atmos. Environ., 70, 454–467,

642   doi:10.1016/J.ATMOSENV.2012.12.036, 2013.

643   Fadnavis, S., Semeniuk, K., Pozzoli, L., Schultz, M. G., Ghude, S. D., Das, S. and Kakatkar, R.: Transport of

644   aerosols into the UTLS and their impact on the Asian monsoon region as seen in a global model simulation,

645   Atmos. Chem. Phys., 13(17), 8771–8786, doi:10.5194/acp-13-8771-2013, 2013.

646   Fast, J. D., Gustafson Jr., W. I., Easter, R. C., Zaveri, R. A., Barnard, J. C., Chapman, E. G., Grell, G. A. and

Peckham, S. E.: Evolution of ozone, particulates, and aerosol direct radiative forcing in the vicinity of Houston using a fully coupled meteorology-chemistry-aerosol model, J. Geophys. Res. Atmos., 111(D21), doi:10.1029/2005JD006721, 2006.

Field, P. R., Möhler, O., Connolly, P., Krämer, M., Cotton, R., Heymsfield, A. J., Saathoff, H. and Schnaiter, M.: Some ice nucleation characteristics of Asian and Saharan desert dust, Atmos. Chem. Phys., 6(10), 2991–3006, doi:10.5194/acp-6-2991-2006, 2006.

Giannakopoulou, E. M. and Toumi, R.: The Persian Gulf summertime low-level jet over sloping terrain, Q. J. R. Meteorol. Soc., 138(662), 145–157, doi:10.1002/qj.901, 2012.

Ginoux, P., Chin, M., Tegen, I., Prospero, J. M., Holben, B., Dubovik, O. and Lin, S.-J.: Sources and distributions of dust aerosols simulated with the GOCART model, J. Geophys. Res. Atmos., 106(D17), 20255–20273, doi:10.1029/2000JD000053, 2001.

Ginoux, P., Prospero, J. M., Gill, T. E., Hsu, N. C. and Zhao, M.: Global-scale attribution of anthropogenic and natural dust sources and their emission rates based on MODIS Deep Blue aerosol products, Rev. Geophys., 50(3), doi:10.1029/2012RG000388, 2012.

Grell, G. A., Peckham, S. E., Schmitz, R., McKeen, S. A., Frost, G., Skamarock, W. C. and Eder, B.: Fully coupled "online" chemistry within the WRF model, Atmos. Environ., 39(37), 6957–6975, doi:10.1016/J.ATMOSENV.2005.04.027, 2005.

Hasanean, H., Almazroui, M., Hasanean, H. and Almazroui, M.: Rainfall: Features and Variations over Saudi Arabia, A Review, Climate, 3(3), 578–626, doi:10.3390/cli3030578, 2015.

Haywood, J. M., Allan, R. P., Culverwell, I., Slingo, T., Milton, S., Edwards, J. and Clerbaux, N.: Can desert dust explain the outgoing longwave radiation anomaly over the Sahara during July 2003?, J. Geophys. Res. Atmos., 110(D5), doi:10.1029/2004JD005232, 2005.

Heald, C. L., Ridley, D. A., Kroll, J. H., Barrett, S. R. H., Cady-Pereira, K. E., Alvarado, M. J. and Holmes, C. D.: Contrasting the direct radiative effect and direct radiative forcing of aerosols, Atmos. Chem. Phys., 14(11), 5513–5527, doi:10.5194/acp-14-5513-2014, 2014.

Heinold, B., Knippertz, P., Marsham, J. H., Fiedler, S., Dixon, N. S., Schepanski, K., Laurent, B. and Tegen, I.: The role of deep convection and nocturnal low-level jets for dust emission in summertime West Africa: Estimates from convection-permitting simulations, J. Geophys. Res. Atmos., 118(10), 4385–4400, doi:10.1002/jgrd.50402, 2013.

Huneeus, N., Schulz, M., Balkanski, Y., Griesfeller, J., Prospero, J., Kinne, S., Bauer, S., Boucher, O., Chin, M., Dentener, F., Diehl, T., Easter, R., Fillmore, D., Ghan, S., Ginoux, P., Grini, A., Horowitz, L., Koch, D., Krol, M. C., Landing, W., Liu, X., Mahowald, N., Miller, R., Morcrette, J.-J., Myhre, G., Penner, J., Perlwitz, J., Stier, P., Takemura, T. and Zender, C. S.: Global dust model intercomparison in AeroCom phase I, Atmos. Chem. Phys., 11(15), 7781–7816, doi:10.5194/acp-11-7781-2011, 2011.

Jickells, T. and Moore, C. M.: The Importance of Atmospheric Deposition for Ocean Productivity, Annu. Rev. Ecol. Evol. Syst., 46(1), 481–501, doi:10.1146/annurev-ecolsys-112414-054118, 2015.

Jish Prakash, P., Stenchikov, G., Kalenderski, S., Osipov, S. and Bangalath, H.: The impact of dust storms on the

Arabian Peninsula and the Red Sea, Atmos. Chem. Phys., 15(1), 199–222, doi:10.5194/acp-15-199-2015, 2015.

Jung, E., Shao, Y. and Sakai, T.: A study on the effects of convective transport on regional-scale Asian dust storms in 2002, J. Geophys. Res. Atmos., 110(D20), doi:10.1029/2005JD005808, 2005.

Kain, J. S.: The Kain–Fritsch Convective Parameterization: An Update, J. Appl. Meteorol., 43(1), 170–181, doi:10.1175/1520-0450(2004)043<0170:TKCPAU>2.0.CO;2, 2004.

Kalenderski, S., Stenchikov, G. and Zhao, C.: Modeling a typical winter-time dust event over the Arabian Peninsula and the Red Sea, Atmos. Chem. Phys., 13(4), 1999–2014, doi:10.5194/acp-13-1999-2013, 2013.

Kalenderski, S. and Stenchikov, G.: High-resolution regional modeling of summertime transport and impact of African dust over the Red Sea and Arabian Peninsula, J. Geophys. Res. Atmos., 121(11), 6435–6458, doi:10.1002/2015JD024480, 2016.

Karydis, V. A., Kumar, P., Barahona, D., Sokolik, I. N. and Nenes, A.: On the effect of dust particles on global cloud condensation nuclei and cloud droplet number, J. Geophys. Res. Atmos., 116(D23), doi:10.1029/2011JD016283, 2011.

Kinne, S., Lohmann, U., Feichter, J., Schulz, M., Timmreck, C., Ghan, S., Easter, R., Chin, M., Ginoux, P., Takemura, T., Tegen, I., Koch, D., Herzog, M., Penner, J., Pitari, G., Holben, B., Eck, T., Smirnov, A., Dubovik, O., Slutsker, I., Tanre, D., Torres, O., Mishchenko, M., Geogdzhayev, I., Chu, D. A. and Kaufman, Y.: Monthly averages of aerosol properties: A global comparison among models, satellite data, and AERONET ground data, J. Geophys. Res. Atmos., 108(D20), doi:10.1029/2001JD001253, 2003.

Kishcha, P., Alpert, P., Barkan, J., Kirschner, I. and Machenhauer, B.: Atmospheric response to Saharan dust deduced from ECMWF reanalysis (ERA) temperature increments, Tellus B Chem. Phys. Meteorol., 55(4), 901–913, doi:10.3402/tellusb.v55i4.16380, 2011.

Klich, C. A. and Fuelberg, H. E.: The role of horizontal model resolution in assessing the transport of CO in a middle latitude cyclone using WRF-Chem, Atmos. Chem. Phys., 14(2), 609–627, doi:10.5194/acp-14-609-2014, 2014.

Klose, M. and Shao, Y.: Stochastic parameterization of dust emission and application to convective atmospheric conditions, Atmos. Chem. Phys., 12, 7309-7320, doi:10.5194/acp-12-7309-2012, 2012.

Knopf, D. A. and Koop, T.: Heterogeneous nucleation of ice on surrogates of mineral dust, J. Geophys. Res. Atmos., 111(D12), doi:10.1029/2005JD006894, 2006.

Kok, J. F., Mahowald, N. M., Fratini, G., Gillies, J. A., Ishizuka, M., Leys, J. F., Mikami, M., Park, M.-S., Park, S.-U., Van Pelt, R. S. and Zobeck, T. M.: An improved dust emission model – Part 1: Model description and comparison against measurements, Atmos. Chem. Phys., 14(23), 13023–13041, doi:10.5194/acp-14-13023-2014, 2014.

Kok, J. F., Ward, D. S., Mahowald, N. M. and Evan, A. T.: Global and regional importance of the direct dust-climate feedback, Nat. Commun., 9(1), 241, doi:10.1038/s41467-017-02620-y, 2018.

Largeron, Y., Guichard, F., Bouniol, D., Couvreux, F., Kergoat, L. and Marticorena, B.: Can we use surface wind

fields from meteorological reanalyses for Sahelian dust emission simulations?, Geophys. Res. Lett., 42(7), 2490–2499, doi:10.1002/2014GL062938, 2015.

Lee, Y. H., Chen, K. and Adams, P. J.: Development of a global model of mineral dust aerosol microphysics, Atmos. Chem. Phys., 9(7), 2441–2458, doi:10.5194/acp-9-2441-2009, 2009.

Liao, H. and Seinfeld, J. H.: Radiative forcing by mineral dust aerosols: Sensitivity to key variables, J. Geophys. Res. Atmos., 103(D24), 31637–31645, doi:10.1029/1998JD200036, 1998.

Mahowald, N. M., Ballantine, J. A., Feddema, J. and Ramankutty, N.: Global trends in visibility: implications for dust sources, Atmos. Chem. Phys., 7(12), 3309–3339, doi:10.5194/acp-7-3309-2007, 2007.

Mahowald, N. M., Baker, A. R., Bergametti, G., Brooks, N., Duce, R. A., Jickells, T. D., Kubilay, N., Prospero, J. M. and Tegen, I.: Atmospheric global dust cycle and iron inputs to the ocean, Global Biogeochem. Cycles, 19(4), doi:10.1029/2004GB002402, 2005.

Manktelow, P. T., Carslaw, K. S., Mann, G. W. and Spracklen, D. V: The impact of dust on sulfate aerosol, CN and CCN during an East Asian dust storm, Atmos. Chem. Phys., 10(2), 365–382, doi:10.5194/acp-10-365-2010, 2010.

Marsham, J. H., Parker, D. J., Grams, C. M., Taylor, C. M. and Haywood, J. M.: Uplift of Saharan dust south of the intertropical discontinuity, J. Geophys. Res. Atmos., 113(D21), doi:10.1029/2008JD009844, 2008.

Marsham, J. H., Knippertz, P., Dixon, N. S., Parker, D. J. and Lister, G. M. S.: The importance of the representation of deep convection for modeled dust-generating winds over West Africa during summer, Geophys. Res. Lett., 38(16), doi:10.1029/2011GL048368, 2011.

Marticorena, B. and Bergametti, G.: Modeling the atmospheric dust cycle: 1. Design of a soil-derived dust emission scheme, J. Geophys. Res. Atmos., 100(D8), 16415–16430, doi:10.1029/95JD00690, 1995.

Martin, J. H.: Iron still comes from above, Nature, 353(6340), 123, doi:10.1038/353123b0, 1991.

Menut, L.: Sensitivity of hourly Saharan dust emissions to NCEP and ECMWF modeled wind speed, J. Geophys. Res. Atmos., 113(D16), doi:10.1029/2007JD009522, 2008.

Miller, S. D., Grasso, L., Bian, Q., Kreidenweis, S., Dostalek, J., Solbrig, J., Bukowski, J., van den Heever, S. C., Wang, Y., Xu, X., Wang, J., Walker, A., Wu, T.-C., Zupanski, M., Chiu, C., and Reid, J.: *A Tale of Two Dust Storms*: Analysis of a Complex Dust Event in the Middle East, Atmos. Meas. Tech. Discuss., doi:10.5194/amt-2019-82, 2019.

Miller, S. D., Kuciauskas, A. P., Liu, M., Ji, Q., Reid, J. S., Breed, D. W., Walker, A. L. and Mandoos, A. Al: Haboob dust storms of the southern Arabian Peninsula, J. Geophys. Res. Atmos., 113(D1), doi:10.1029/2007JD008550, 2008.

Morrison, H., Curry, J. A. and Khvorostyanov, V. I.: A New Double-Moment Microphysics Parameterization for Application in Cloud and Climate Models. Part I: Description, J. Atmos. Sci., 62(6), 1665–1677, doi:10.1175/JAS3446.1, 2005.

Morrison, H., Thompson, G. and Tatarskii, V.: Impact of Cloud Microphysics on the Development of Trailing Stratiform Precipitation in a Simulated Squall Line: Comparison of One- and Two-Moment Schemes, Mon. Weather Rev., 137(3), 991–1007, doi:10.1175/2008MWR2556.1, 2009.

757   Nakanishi, M. and Niino, H.: An Improved Mellor--Yamada Level-3 Model: Its Numerical Stability and Application

758   to a Regional Prediction of Advection Fog, Boundary-Layer Meteorol., 119(2), 397–407,

759   doi:10.1007/s10546-005-9030-8, 2006.

760   Nakanishi, M. and NIINO, H.: Development of an Improved Turbulence Closure Model for the Atmospheric

761   Boundary Layer, J. Meteorol. Soc. Japan. Ser. II, 87(5), 895–912, doi:10.2151/jmsj.87.895, 2009.

762   National Centers for Environmental Prediction/National Weather Service/NOAA/U.S. Department of Commerce:

763   NCEP GDAS/FNL 0.25 Degree Global Tropospheric Analyses and Forecast Grids, Research Data Archive

764   at the National Center for Atmospheric Research, Computational and Information Systems Laboratory,

765   Boulder, CO, https://doi.org/10.5065/D65Q4T4Z, 2015.

766   Niu, G.-Y., Yang, Z.-L., Mitchell, K. E., Chen, F., Ek, M. B., Barlage, M., Kumar, A., Manning, K., Niyogi, D.,

767   Rosero, E., Tewari, M. and Xia, Y.: The community Noah land surface model with multiparameterization

768   options (Noah-MP): 1. Model description and evaluation with local-scale measurements, J. Geophys. Res.

769   Atmos., 116(D12), doi:10.1029/2010JD015139, 2011.

770   Pantillon, F., Knippertz, P., Marsham, J. H. and Birch, C. E.: A Parameterization of Convective Dust Storms for

771   Models with Mass-Flux Convection Schemes, J. Atmos. Sci., 72(6), 2545–2561, doi:10.1175/JAS-D-14-

772   0341.1, 2015.

773   Pantillon, F., Knippertz, P., Marsham, J. H., Panitz, H.-J. and Bischoff-Gauss, I.: Modeling haboob dust storms in

774   large-scale weather and climate models, J. Geophys. Res. Atmos., 121(5), 2090–2109,

775   doi:10.1002/2015JD024349, 2016.

776   Pérez, C., Nickovic, S., Pejanovic, G., Baldasano, J. M. and Özsoy, E.: Interactive dust-radiation modeling: A step

777   to improve weather forecasts, J. Geophys. Res. Atmos., 111(D16), doi:10.1029/2005JD006717, 2006.

778   Pope, R. J., Marsham, J. H., Knippertz, P., Brooks, M. E. and Roberts, A. J.: Identifying errors in dust models from

779   data assimilation, Geophys. Res. Lett., 43(17), 9270–9279, doi:10.1002/2016GL070621, 2016.

780   Prospero, J. M.: Long-term measurements of the transport of African mineral dust to the southeastern United States:

781   Implications for regional air quality, J. Geophys. Res. Atmos., 104(D13), 15917–15927,

782   doi:10.1029/1999JD900072, 1999.

783   Reid, J. S., Benedetti, A., Colarco, P. R. and Hansen, J. A.: International Operational Aerosol Observability

784   Workshop, Bull. Am. Meteorol. Soc., 92(6), ES21-ES24, doi:10.1175/2010BAMS3183.1, 2010.

785   Reinfried, F., Tegen, I., Heinold, B., Hellmuth, O., Schepanski, K., Cubasch, U., Huebener, H. and Knippertz, P.:

786   Simulations of convectively-driven density currents in the Atlas region using a regional model: Impacts on

787   dust emission and sensitivity to horizontal resolution and convection schemes, J. Geophys. Res. Atmos.,

788   114(D8), doi:10.1029/2008JD010844, 2009.

789   Ridley, D. A., Heald, C. L., Pierce, J. R. and Evans, M. J.: Toward resolution-independent dust emissions in global

790   models: Impacts on the seasonal and spatial distribution of dust, Geophys. Res. Lett., 40(11), 2873–2877,

791   doi:10.1002/grl.50409, 2013.

792   Roberts, A. J., Woodage, M. J., Marsham, J. H., Highwood, E. J., Ryder, C. L., McGinty, W., Wilson, S., and

793   Crook, J.: Can explicit convection improve modelled dust in summertime West Africa?, Atmos. Chem.
794   Phys., 18, 9025-9048, https://doi.org/10.5194/acp-18-9025-2018, 2018.

795 Saleeby, S. M., van den Heever, S. C., Bukowski, J., Walker, A. L., Solbrig, J. E., Atwood, S. A., Bian, Q.,
796   Kreidenweis, S. M., Wang, Y., Wang, J. and Miller, S. D.: The Influence of Simulated Surface Dust
797   Lofting Erodible Fraction on Radiative Forcing, Atmos. Chem. Phys. Discuss., 2019, 1–35,
798   doi:10.5194/acp-2018-1302, 2019.

799 Schepanski, K., Knippertz, P., Fiedler, S., Timouk, F. and Demarty, J.: The sensitivity of nocturnal low-level jets
800   and near-surface winds over the Sahel to model resolution, initial conditions and boundary-layer set-up.
801   Q.J.R. Meteorol. Soc., 141, 1442-1456. doi:10.1002/qj.2453, 2015.

802 Seigel, R. B. and van den Heever, S. C.: Dust Lofting and Ingestion by Supercell Storms, J. Atmos. Sci., 69(5),
803   1453–1473, doi:10.1175/JAS-D-11-0222.1, 2012.

804 Sessions, W. R., Reid, J. S., Benedetti, A., Colarco, P. R., da Silva, A., Lu, S., Sekiyama, T., Tanaka, T. Y.,
805   Baldasano, J. M., Basart, S., Brooks, M. E., Eck, T. F., Iredell, M., Hansen, J. A., Jorba, O. C., Juang, H.-
806   M. H., Lynch, P., Morcrette, J.-J., Moorthi, S., Mulcahy, J., Pradhan, Y., Razinger, M., Sampson, C. B.,
807   Wang, J. and Westphal, D. L.: Development towards a global operational aerosol consensus: basic
808   climatological characteristics of the International Cooperative for Aerosol Prediction Multi-Model
809   Ensemble (ICAP-MME), Atmos. Chem. Phys., 15(1), 335–362, doi:10.5194/acp-15-335-2015, 2015.

810 Shwehdi, M. H.: Thunderstorm distribution and frequency in Saudi Arabia, J. Geophys. Eng., 2(3), 252–267,
811   doi:10.1088/1742-2132/2/3/009, 2005.

812 Skamarock, W. C., Klemp, J. B., Dudhia, J. O. G. D., and Barker, D. M.: A description of the Advanced Research
813   WRF version 3, NCAR Tech. Note NCAR/TN-4751STR, NCAR, http://dx.doi.org/10.5065/D68S4MVH,
814   Boulder, CO, 2008.

815 Slingo, A., Ackerman, T. P., Allan, R. P., Kassianov, E. I., McFarlane, S. A., Robinson, G. J., Barnard, J. C., Miller,
816   M. A., Harries, J. E., Russell, J. E. and Dewitte, S.: Observations of the impact of a major Saharan dust
817   storm on the atmospheric radiation balance, Geophys. Res. Lett., 33(24), doi:10.1029/2006GL027869,
818   2006.

819 Sokolik, I. N. and Toon, O. B.: Direct radiative forcing by anthropogenic airborne mineral aerosols, Nature,
820   381(6584), 681–683, doi:10.1038/381681a0, 1996.

821 Stafoggia, M., Zauli-Sajani, S., Pey, J., Samoli, E., Alessandrini, E., Basagaña, X., Cernigliaro, A., Chiusolo, M.,
822   Demaria, M., Díaz, J., Faustini, A., Katsouyanni, K., Kelessis, A. G., Linares, C., Marchesi, S., Medina, S.,
823   Pandolfi, P., Pérez, N., Querol, X., Randi, G., Ranzi, A., Tobias, A., Forastiere, F. and null null: Desert
824   Dust Outbreaks in Southern Europe: Contribution to Daily PM_{10} Concentrations and Short-Term
825   Associations with Mortality and Hospital Admissions, Environ. Health Perspect., 124(4), 413–419,
826   doi:10.1289/ehp.1409164, 2016.

827 Stephens, G. L., L'Ecuyer, T., Forbes, R., Gettelmen, A., Golaz, J.-C., Bodas-Salcedo, A., Suzuki, K., Gabriel, P.,
828   and Haynes, J.: Dreary state of precipitation in global models, J. Geophys. Res., 115, D24211,
829   doi:10.1029/2010JD014532, 2010.

830   Sun, Y., Solomon, S., Dai, A., and Portmann, R. W.: How often does it rain? J. Clim., 19, 916–934,
831   doi:10.1175/JCLI3672.1, 2006.

832   Takemi, T.: Importance of the Numerical Representation of Shallow and Deep Convection for Simulations of
833   Dust Transport over a Desert Region, Adv. Meteorol., vol. 2012, 1-13, doi: 10.1155/2012/413584, 2012.

834   Tanaka, T. Y. and Chiba, M.: A numerical study of the contributions of dust source regions to the global dust
835   budget, Glob. Planet. Change, 52(1–4), 88–104, doi:10.1016/J.GLOPLACHA.2006.02.002, 2006.

836   Tegen, I. and Lacis, A. A.: Modeling of particle size distribution and its influence on the radiative properties of
837   mineral dust aerosol, J. Geophys. Res. Atmos., 101(D14), 19237–19244, doi:10.1029/95JD03610, 1996.

838   Teixeira, J. C., Carvalho, A. C., Tuccella, P., Curci, G. and Rocha, A.: WRF-chem sensitivity to vertical resolution
839   during a saharan dust event, Phys. Chem. Earth, Parts A/B/C, 94, 188–195,
840   doi:10.1016/J.PCE.2015.04.002, 2016.

841   Todd, M. C., Bou Karam, D., Cavazos, C., Bouet, C., Heinold, B., Baldasano, J. M., Cautenet, G., Koren, I., Perez,
842   C., Solmon, F., Tegen, I., Tulet, P., Washington, R. and Zakey, A.: Quantifying uncertainty in estimates of
843   mineral dust flux: An intercomparison of model performance over the Bodélé Depression, northern Chad, J.
844   Geophys. Res. Atmos., 113(D24), doi:10.1029/2008JD010476, 2008.

845   Tulet, P., Crahan-Kaku, K., Leriche, M., Aouizerats, B. and Crumeyrolle, S.: Mixing of dust aerosols into a
846   mesoscale convective system: Generation, filtering and possible feedbacks on ice anvils, Atmos. Res.,
847   96(2–3), 302–314, doi:10.1016/J.ATMOSRES.2009.09.011, 2010.

848   Twohy, C. H., Kreidenweis, S. M., Eidhammer, T., Browell, E. V, Heymsfield, A. J., Bansemer, A. R., Anderson, B.
849   E., Chen, G., Ismail, S., DeMott, P. J. and Van Den Heever, S. C.: Saharan dust particles nucleate droplets
850   in eastern Atlantic clouds, Geophys. Res. Lett., 36(1), doi:10.1029/2008GL035846, 2009.

851   Uno, I., Wang, Z., Chiba, M., Chun, Y. S., Gong, S. L., Hara, Y., Jung, E., Lee, S.-S., Liu, M., Mikami, M., Music,
852   S., Nickovic, S., Satake, S., Shao, Y., Song, Z., Sugimoto, N., Tanaka, T. and Westphal, D. L.: Dust model
853   intercomparison (DMIP) study over Asia: Overview, J. Geophys. Res. Atmos., 111(D12),
854   doi:10.1029/2005JD006575, 2006.

855   van Donkelaar, A., Martin, R. V, Brauer, M., Kahn, R., Levy, R., Verduzco, C. and Villeneuve, P. J.: Global
856   estimates of ambient fine particulate matter concentrations from satellite-based aerosol optical depth:
857   development and application, Environ. Health Perspect., 118(6), 847–855, doi:10.1289/ehp.0901623, 2010.

858   Woodage, M. J. and Woodward, S.: U.K. HiGEM: Impacts of Desert Dust Radiative Forcing in a High-Resolution
859   Atmospheric GCM, J. Clim., 27(15), 5907–5928, doi:10.1175/JCLI-D-13-00556.1, 2014.

860   Yang, Q., Easter, R. C., Campuzano-Jost, P., Jimenez, J. L., Fast, J. D., Ghan, S. J., Wang, H., Berg, L. K., Barth,
861   M. C., Liu, Y., Shrivastava, M. B., Singh, B., Morrison, H., Fan, J., Ziegler, C. L., Bela, M., Apel, E.,
862   Diskin, G. S., Mikoviny, T. and Wisthaler, A.: Aerosol transport and wet scavenging in deep convective
863   clouds: A case study and model evaluation using a multiple passive tracer analysis approach, J. Geophys.
864   Res. Atmos., 120(16), 8448–8468, doi:10.1002/2015JD023647, 2015.

865   Yang, Z.-L., Niu, G.-Y., Mitchell, K. E., Chen, F., Ek, M. B., Barlage, M., Longuevergne, L., Manning, K., Niyogi,

866   D., Tewari, M. and Xia, Y.: The community Noah land surface model with multiparameterization options

867   (Noah-MP): 2. Evaluation over global river basins, J. Geophys. Res. Atmos., 116(D12),

868   doi:10.1029/2010JD015140, 2011.

869 Yin, Y., Chen, Q., Jin, L., Chen, B., Zhu, S. and Zhang, X.: The effects of deep convection on the concentration and

870   size distribution of aerosol particles within the upper troposphere: A case study, J. Geophys. Res. Atmos.,

871   117(D22), doi:10.1029/2012JD017827, 2012.

872 Yu, Y., Notaro, M., Kalashnikova, O. V and Garay, M. J.: Climatology of summer Shamal wind in the Middle East,

873   J. Geophys. Res. Atmos., 121(1), 289–305, doi:10.1002/2015JD024063, 2016.

874 Yuter, S. E. and Houze, R. A.: Three-Dimensional Kinematic and Microphysical Evolution of Florida

875   Cumulonimbus. Part II: Frequency Distributions of Vertical Velocity, Reflectivity, and Differential

876   Reflectivity, Mon. Weather Rev., 123(7), 1941–1963, doi:10.1175/1520-

877   0493(1995)123<1941:TDKAME>2.0.CO;2, 1995.

878 Zender, C. S., Miller, R. L. R. L. and Tegen, I.: Quantifying mineral dust mass budgets:Terminology, constraints,

879   and current estimates, Eos, Trans. Am. Geophys. Union, 85(48), 509–512, doi:10.1029/2004EO480002,

880   2004.

881 Zhao, C., Liu, X., Leung, L. R., Johnson, B., McFarlane, S. A., Gustafson Jr., W. I., Fast, J. D. and Easter, R.: The

882   spatial distribution of mineral dust and its shortwave radiative forcing over North Africa: modeling

883   sensitivities to dust emissions and aerosol size treatments, Atmos. Chem. Phys., 10(18), 8821–8838,

884   doi:10.5194/acp-10-8821-2010, 2010.

885

WRF-Chem Version 3.9.1.1	Parameterization / Model Option
Simulation Start	02-Aug-2016-00:00:00 UTC
Simulation End	05-Aug-2016-00:00:00 UTC
Domains	dx = dy = 45km / 15km / 3km
Nesting	One-way
Vertical Levels	50 stretched
Initialization	GDAS-FNL Reanalysis
Aerosol Module / Erodible Grid Map	GOCART / Ginoux et al. (2004)
Microphysics	Morrison 2-Moment
Radiation	RRTMG Longwave & Goddard Shortwave
Land Surface	Noah-MP Land Surface Model
Cumulus Schemes (45 km and 15 km grids only)	Betts–Miller–Janjic (BMJ)
	Kain–Fritsch (KF)
	Grell 3D Ensemble (GD)
	Tiedtke Scheme (TD)
	Simplified Arakawa–Schubert (AS)
Boundary Layer / Surface Layer	MYNN Level 3

886   **Table 1: Summary of WRF-Chem model options utilized and the simulation setup.**
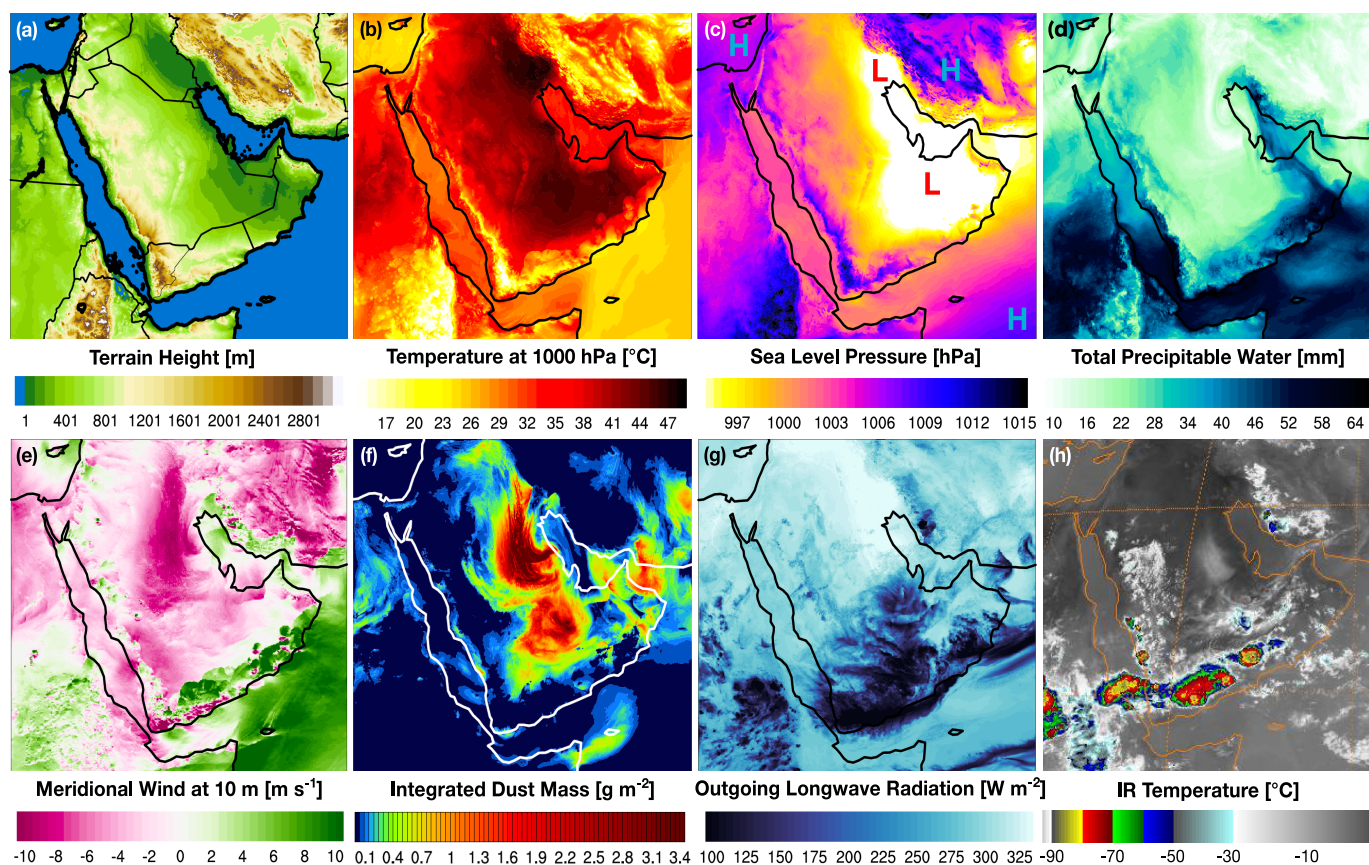
Figure 1: Case study topography and meteorology for August 3, 2016 at 15:00 UTC: (a) terrain height and national boundaries, (b) 1000 hPa Temperature, (c) sea level pressure, (d) total precipitable water, (e) meridional winds at 10 m AGL, (f) vertically integrated dust mass, (g) outgoing longwave radiation, and (h) IR temperature. Panel (h) is observed from Meteosat-7 while panels (a-g) are snapshots from the 3 km WRF-Chem simulation
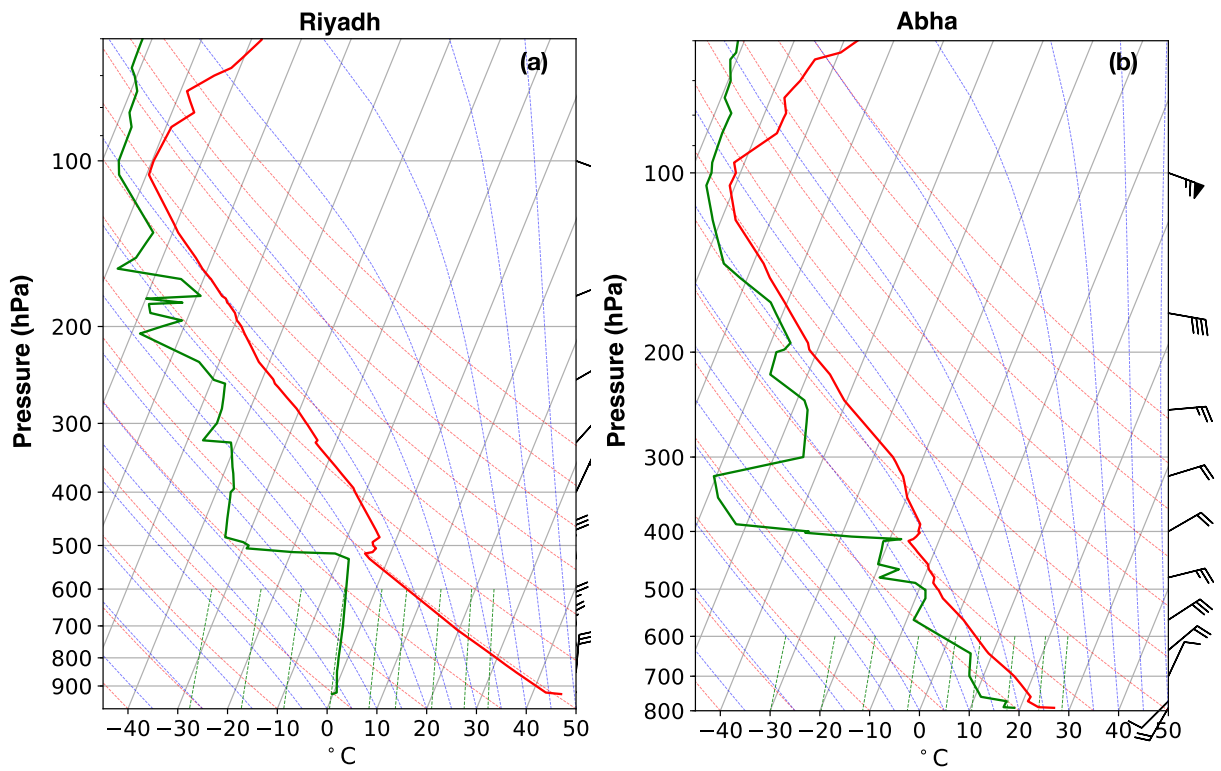
892

893   **Figure 2. Skew-T diagrams for two radiosonde release sites in Saudi Arabia on August 3, 2016 at 12:00 UTC for an inland**
894   **location (a) and a location nearer to the coast (b).**

895

896
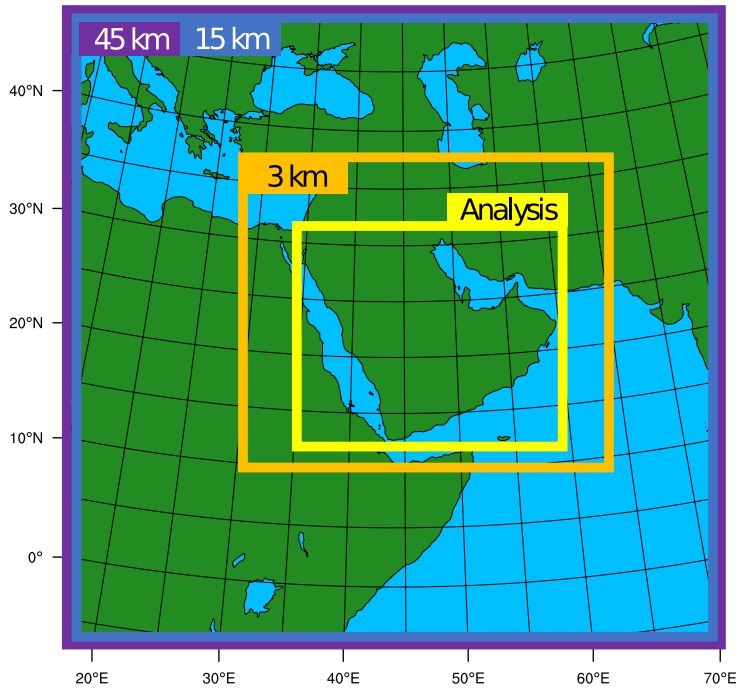
897 **Figure 3: Model domain setup and analysis region for the 45 km (purple) and 15 km (blue) independent simulations with**

898 **cumulus parameterizations, and the 3 km nested convection permitting simulation (orange). The averaging region for the**

899 **analysis is denoted in yellow.**

900
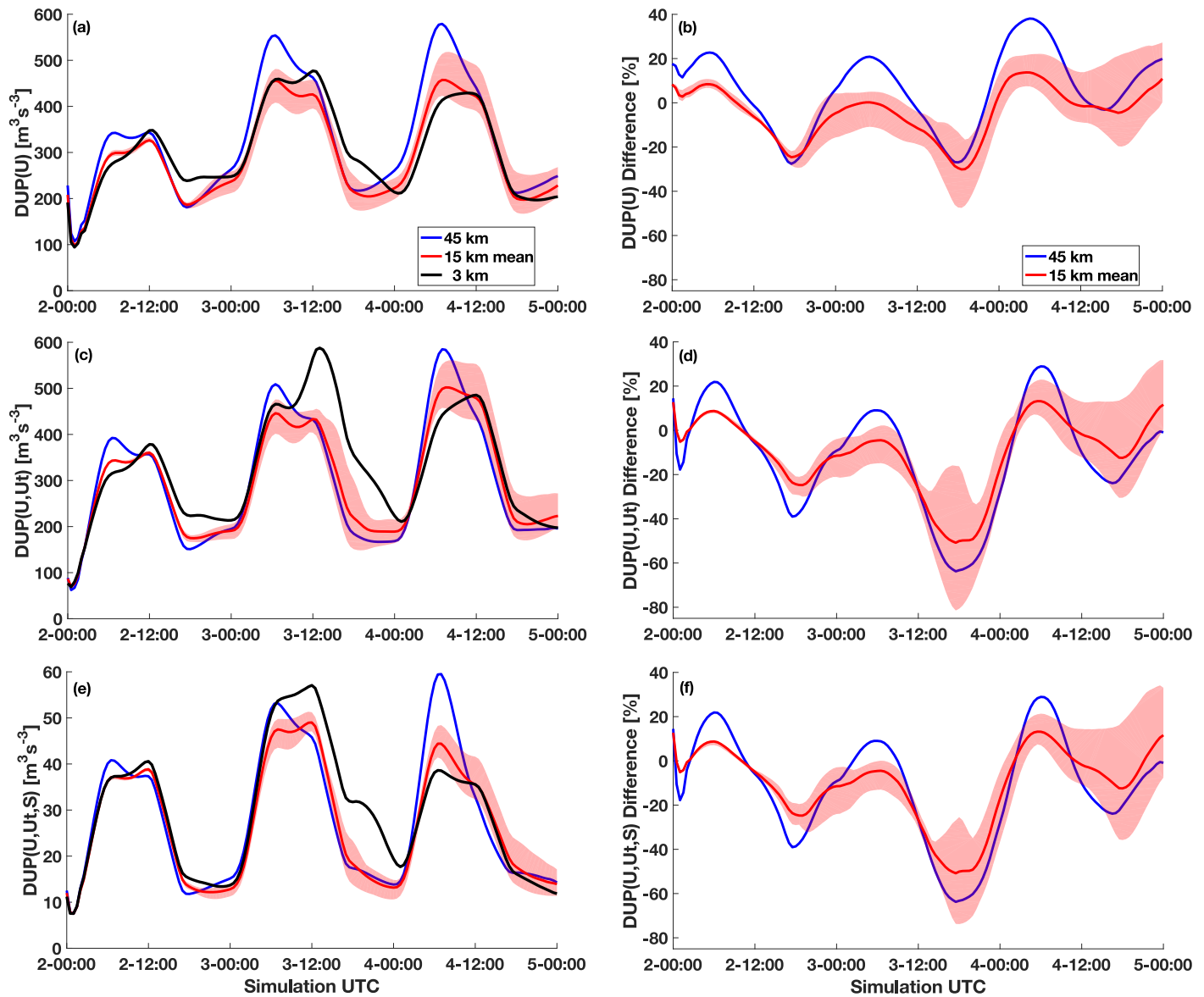
Figure 4: Left column: spatially averaged dust uplift potential for (a) DUP(U), (c) DUP(U,U$_t$), and (e) DUP(U,U$_t$,S) for the

45 km (blue), 15 km mean (red), and 3 km (black) simulations with the maximum and minimum spread across the 15 km

simulations indicated in light red shading. Note that in panel (e) there is a change in scale in the ordinate. Right column:

percent difference between the 3 km convection-permitting simulation and the simulations employing cumulus

parameterizations for the different DUP parameters.

906
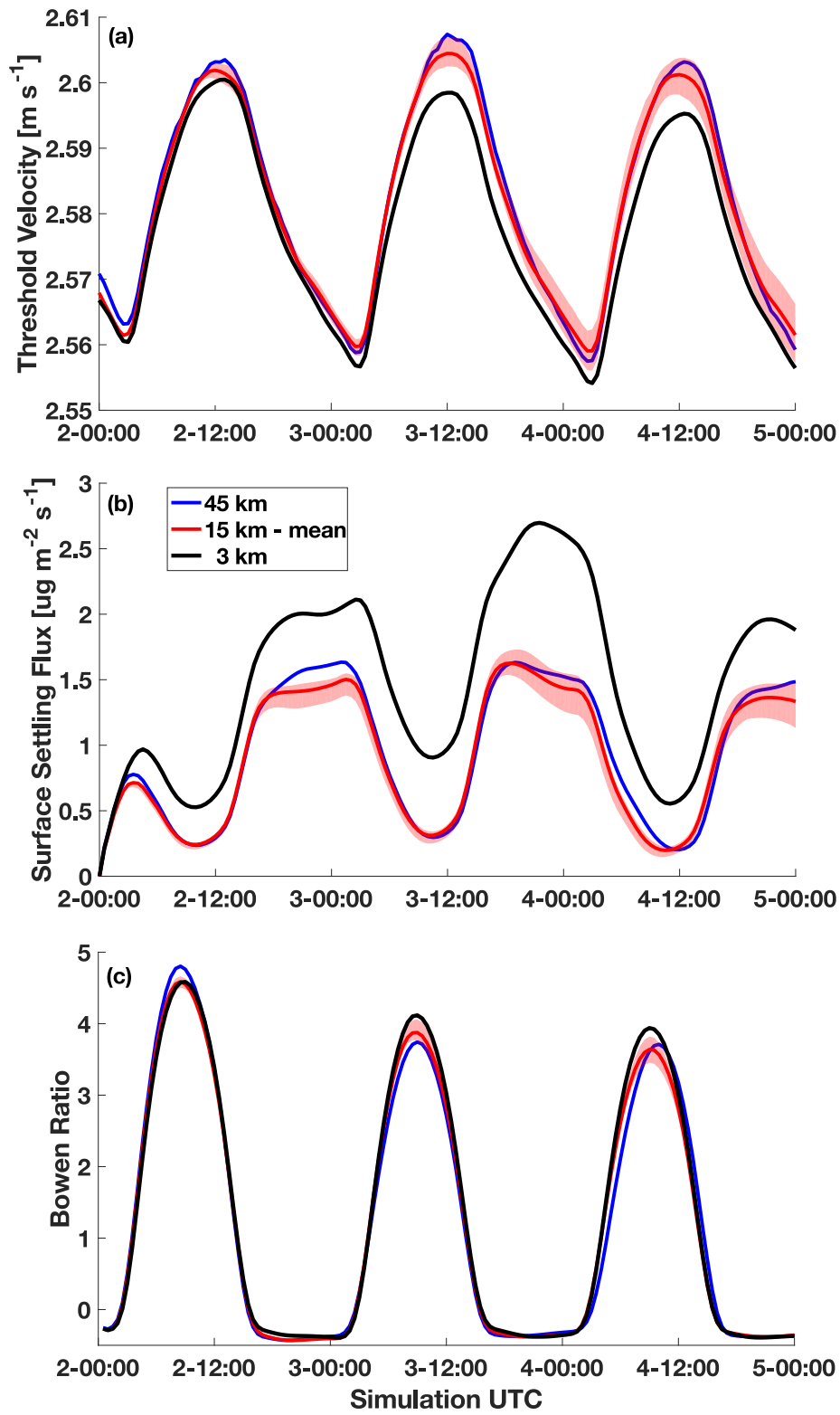
907 **Figure 5: Spatially averaged (a) dust uplift threshold velocity, (b) dust surface settling flux, and (c) Bowen ratio of**

908 **sensible to latent heat flux. Colors and shading are the same as in Fig. 4.**
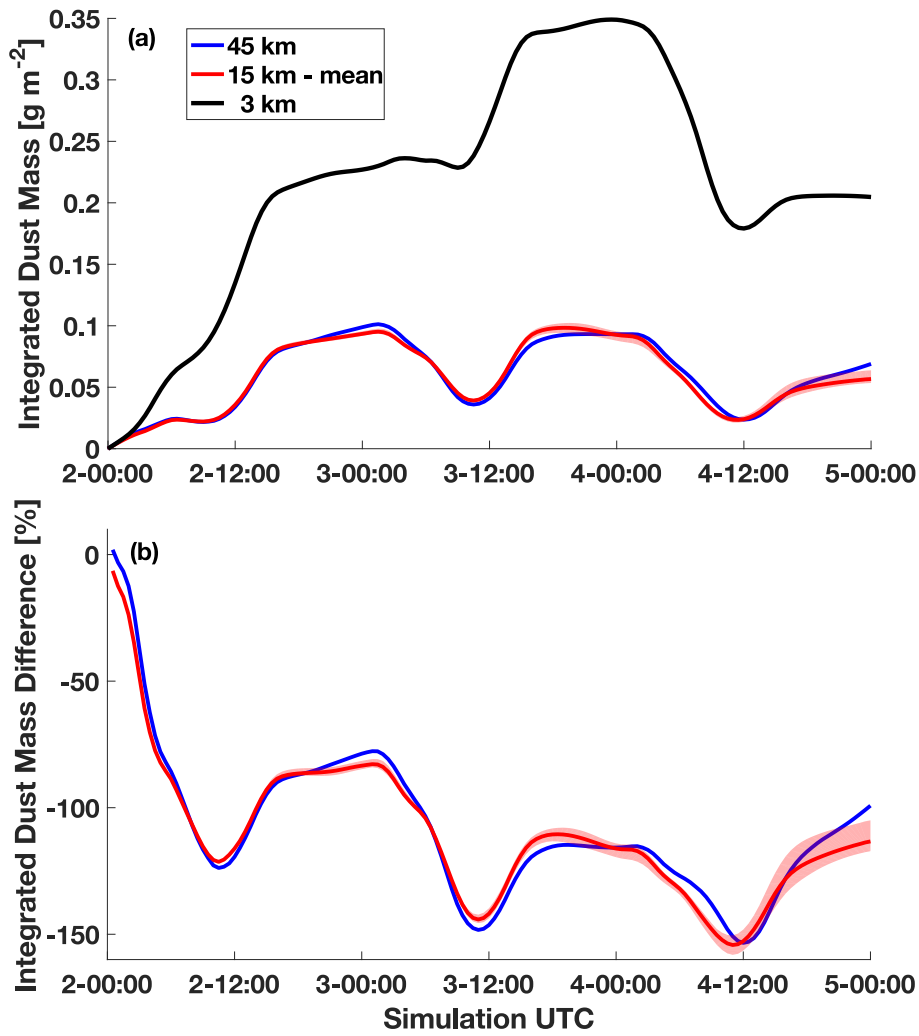
909

910   **Figure 6: Spatially averaged, vertically integrated dust mass. Colors and shading are identical to that in previous figures.**

911
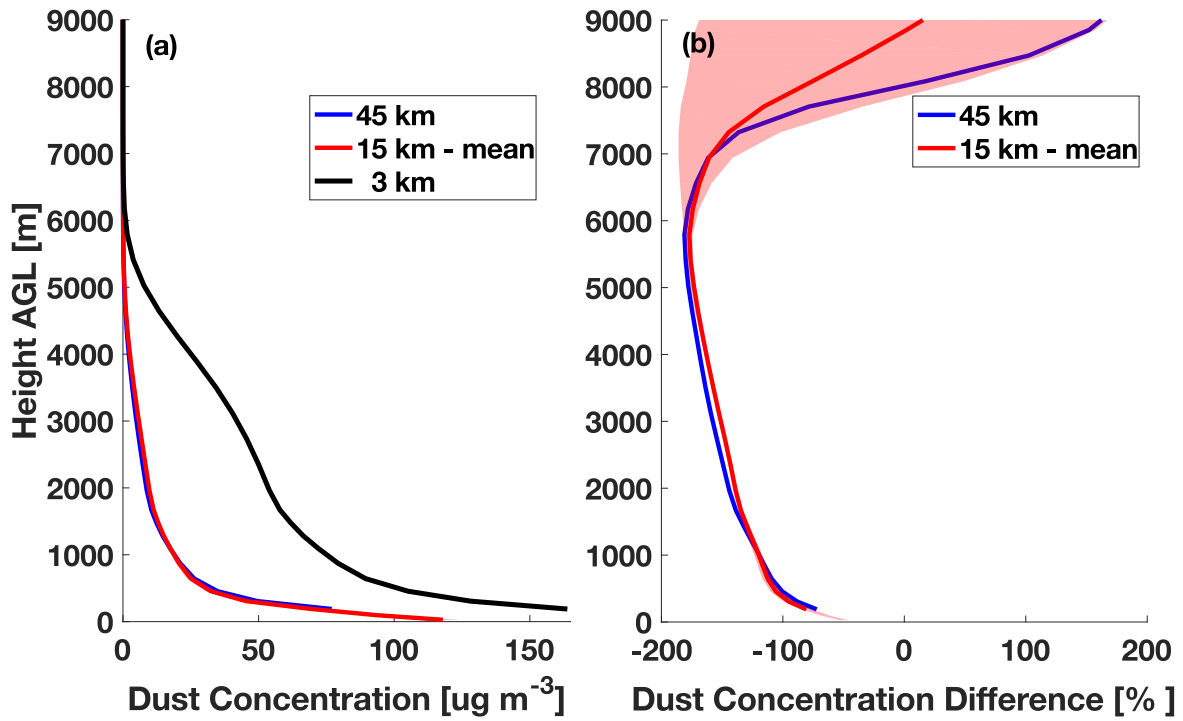
Figure 7: Spatially and time averaged vertical dust concentrations (a), with the (b) percent difference between the 3 km convection-permitting simulation and the simulations employing cumulus parameterizations. Plots are truncated at 9 km since the values above this height do not significantly vary from what is shown here. Colors and shading are identical to that in previous figures.

916
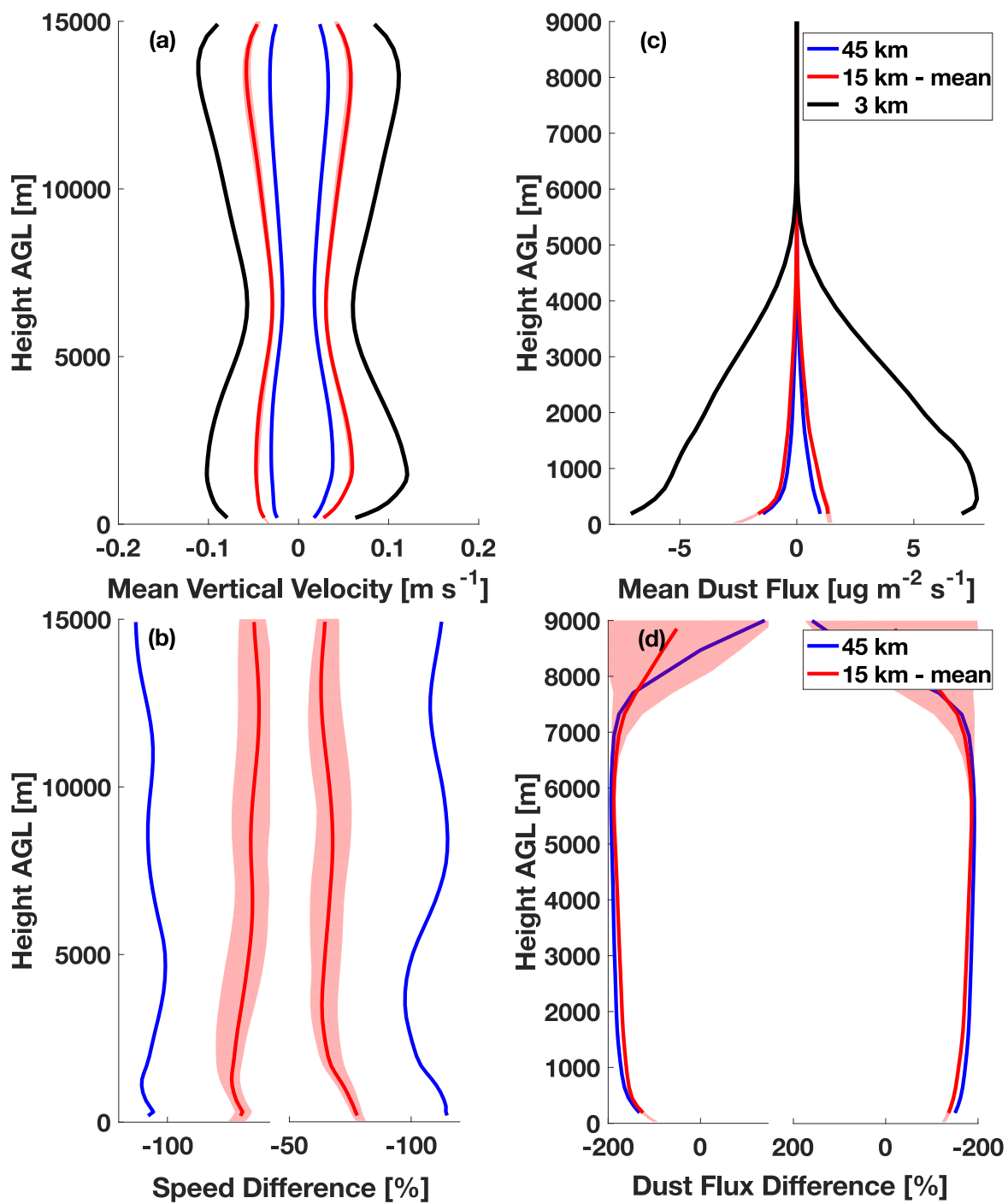
Figure 8. Left column: spatially and time averaged vertical velocities (a), with the (b) percent difference between the 3 km convection-permitting simulation and the simulations employing cumulus parameterizations. All velocities above or below zero were considered. Colors and shading are identical to that in previous figures. Right column: same but for vertical dust mass flux. Note that in panels (c) and (d) the vertical axes are truncated at 9 km since the values above this height do not significantly vary from what is shown here.

922

923
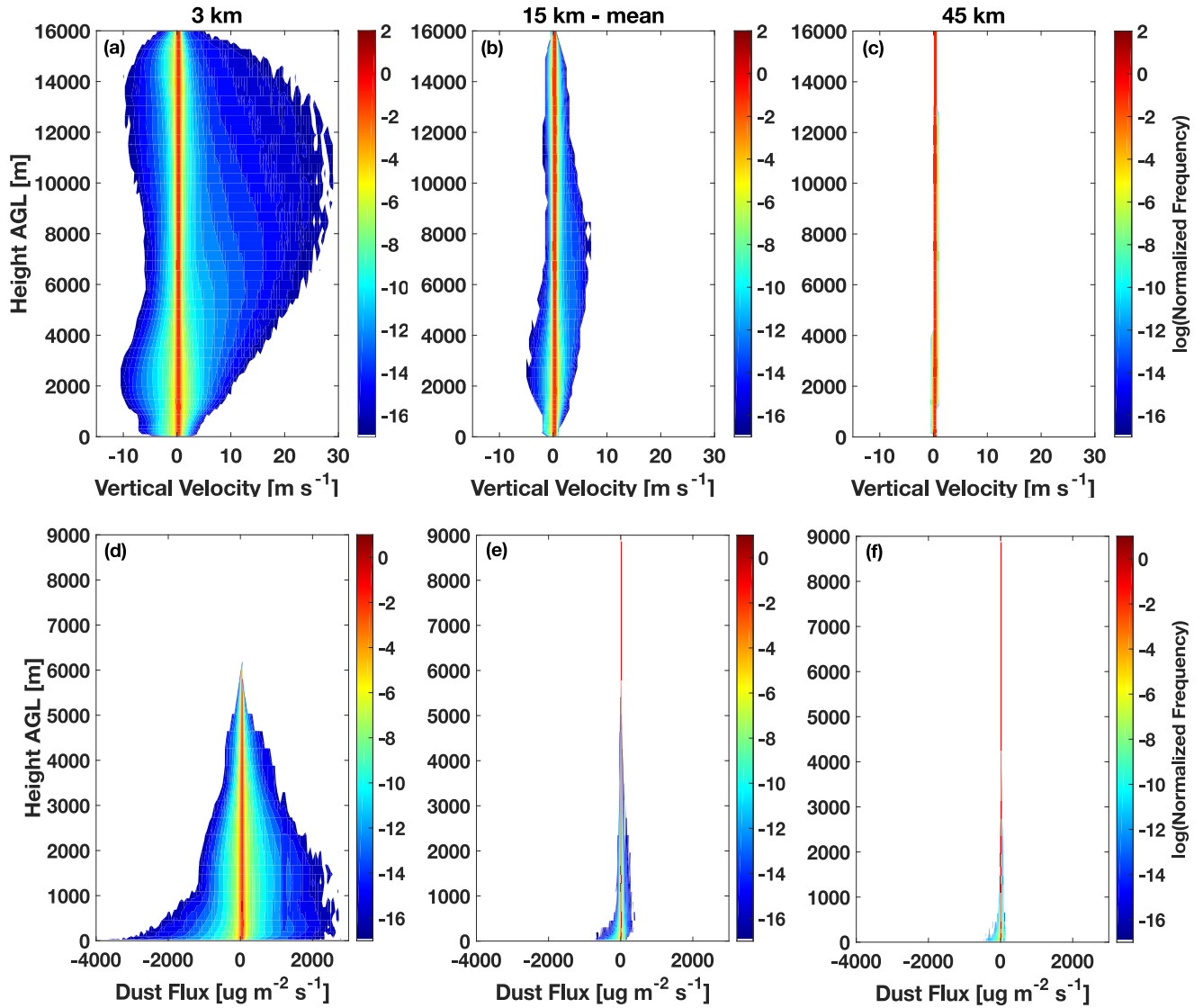
924 **Figure 9: Top row: Contoured Frequency by Altitude Diagrams (CFADs) for vertical velocity, normalized by the number**
925 **of grid points in each respective simulation. The contours are computed on a log scale to highlight the variances away**
926 **from zero. Bottom row: same but for vertical dust mass flux. Note that the panels in the bottom row are truncated at 9**
927 **km since the values above this height do not significantly vary from what is shown here.**

928
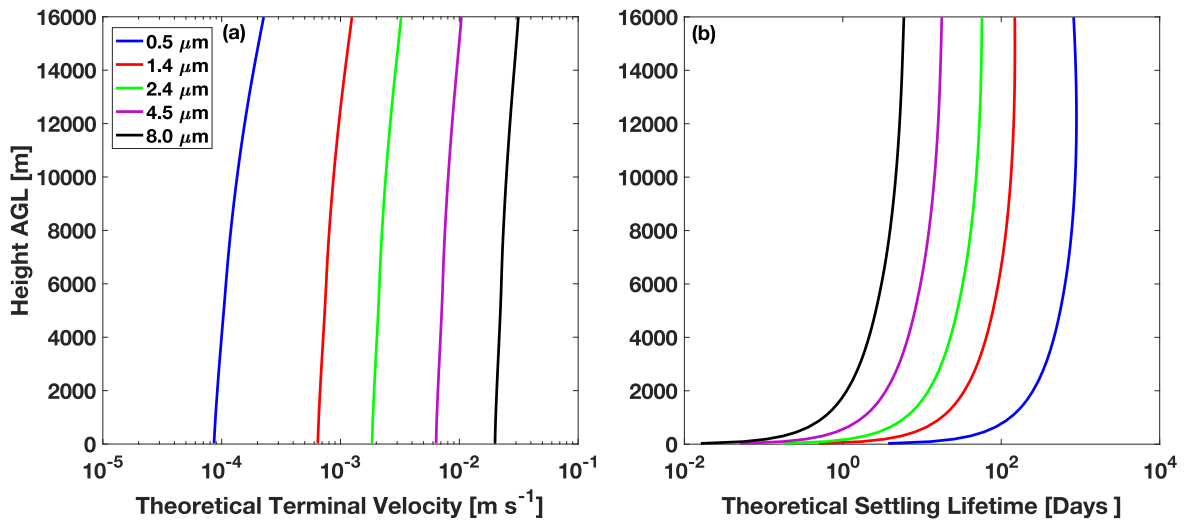
929 **Figure 10: Theoretical terminal velocity of dust particles (a) based on Stokes settling velocity with slip correction for**

930 **pressure dependence for the 5 effective radii of dust particles in WRF-Chem. The calculations assume no vertical**

931 **motions, advection, deposition, coagulation, or condensation. (b) The lifetime of these theoretical dust particles based on**

932 **their height in the atmosphere.**

933

934
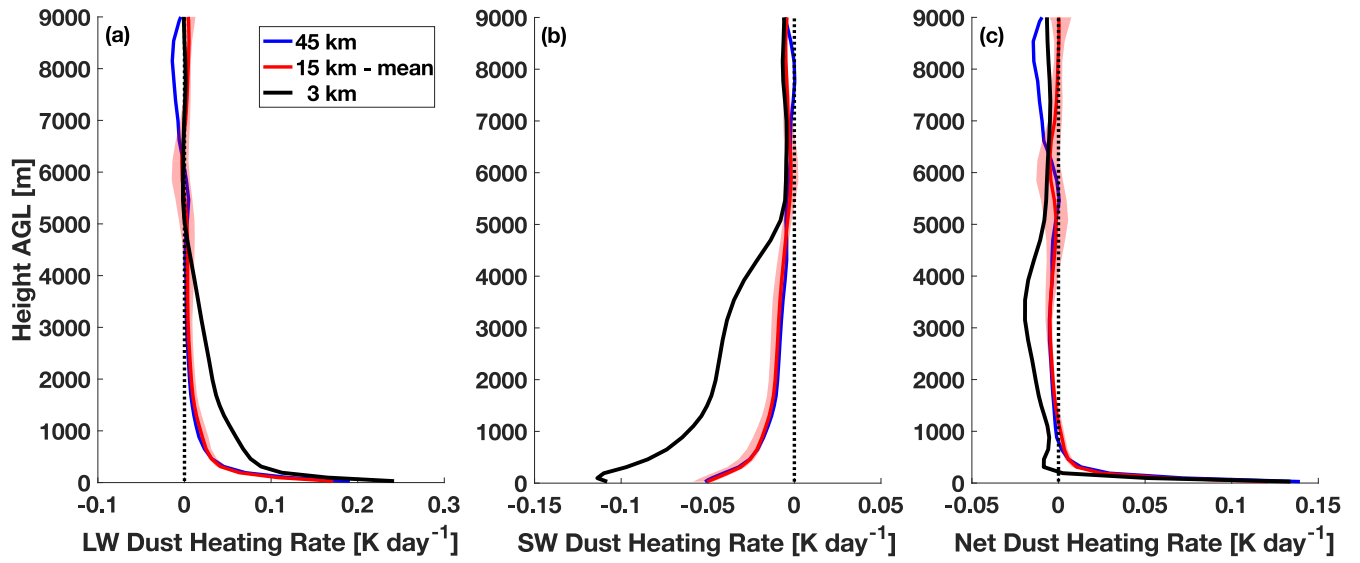
935   **Figure 11: Spatially and time averaged longwave (a), shortwave (b), and net (c) dust heating rate profile for the 45 km**

936   **(blue), 15 km mean (red), and 3 km (black) simulations with the maximum and minimum spread across the 15 km**

937   **simulations indicated in light red shading. Plots are truncated at 9 km since the values above this height do not**

938   **significantly vary from what is shown here.**